Association Euratom - Risø National Laboratory annual progress report 2003

Bindslev, H.; Singh, B.N

Publication date:
2004

Document Version
Publisher's PDF, also known as Version of record

Risø-R-1468(EN)

Association Euratom - Risø National Laboratory Annual Progress Report 2003

Edited by H. Bindslev and B.N. Singh

Risø National Laboratory, Roskilde, Denmark
May 2004

Abstract The programme of the Research Unit of the Fusion Association Euratom - Risø National Laboratory covers work in fusion plasma physics and in fusion technology. The fusion plasma physics research focuses on turbulence and transport, and its interaction with the plasma equilibrium and particles. The effort includes both first principles based modelling, and experimental observations of turbulence and of fast ion dynamics by collective Thomson scattering. The activities in technology cover investigations of radiation damage of fusion reactor materials. These activities contribute to the Next Step, the Long-term and the Underlying Fusion Technology programme. A summary is presented of the results obtained in the Research Unit during 2003.

ISBN 87-550-3347-4 (Internet)
ISSN 0106-2840; 1396-3449

Foreword

Risø participates in the internationally coordinated activities to develop fusion as a major source of energy. The principle being pursued is the fusion of hydrogen isotopes to form helium. This is the process, which powers the sun. To make the fusion process run at a significant rate the hydrogen gas must be heated to high temperatures where it ionises and turns into a plasma. Furthermore, the plasma must be confined to achieve suitable densities and sustain the high temperature. On the sun gravity provides the confinement. On earth, the line we are pursuing, uses a magnetic field for the confinement. While fusion holds the promise of providing a sustainable source of energy, which is environmentally sound, it also presents considerable scientific and engineering challenges. Key issues in the final steps towards realising fusion energy production include:

1. Improving the plasma energy confinement, that is the ratio between the energy of the plasma and the heating power required to sustain the plasma energy. Improving energy confinement implies reducing energy transport out of the plasma, which principally is due to turbulence. So what we really need to do is to understand and control turbulence.
2. Channelling the energy of fast ions, produced in fusion reactions, into heating the bulk plasma without driving turbulence and without premature exit of the fast ions from the plasma. This requires understanding and control of the dynamics of the fast ions in interaction with other particles and with waves.
3. Development of materials, which maintain required mechanical properties under high and sustained neutron fluxes. Neutrons, produced in the fusion reactions, are not confined by the magnetic field. They pass through the first wall of the chamber surrounding the plasma, slowing down on impact with atoms in the wall, thereby giving rise to dislocations in the wall material, which affect the properties of the material.

Risø contributes to fusion research in all these areas: 1) codes, modelling turbulence and transport have been developed and are continually improved, and benchmarked against experiments. 2) Central to understanding the dynamics of fast ions is the acquisition of temporally and spatially resolved measurements of the fast ion velocity distributions in the plasma. Risø, in collaboration with MIT (USA) and European partners, is developing millimetre wave based collective Thomson scattering (CTS) systems for measuring fast ion distributions in current fusion plasmas. Of particular note this year has been Risø's investigation of the feasibility of measuring fast ion dynamics in the next step fusion device, ITER, by CTS. This study, encompassing essentially all potential CTS probe frequencies, found that a millimetre wave system was the best option, that such a system could meet all the measurement requirements set out by the ITER team and it could be built with present or near term technology. 3) In the field of irradiated materials research Risø is investigating the properties of copper alloys relevant to the next step in fusion research, ITER, and of iron alloys, which will be an essential component of a commercial fusion power plant.

Our activities in developing fusion energy are coordinated with the European EURATOM fusion programme through an agreement of association on equal footing with other fusion laboratories in Europe. Our EURATOM association facilitates extensive collaboration with other fusion research laboratories in Europe, crucial in the ongoing build-up of competences at Risø, and gives us access to placing our experimental equipment on large fusion facilities at the Max-Planck Institute for Plasma Physics in Garching and at the Research Centre Jülich, both in Germany. Our association with EURATOM also provides the basis for our participation in the exploitation of the European fusion research centre, JET, located in England. The European fusion programme, with its organisation of programmes at national laboratories as EURATOM associations, is a successful example of a large *European Research Area.*

Henrik Bindslev
Risø National Laboratory
April 2004

Contents

1. Summary of Research Unit activities

The activities in the Research Unit cover two main areas:

Fusion Plasma Physics, which includes:

- *Theoretical and numerical turbulence studies*. Turbulence and the associated anomalous transport is investigated using first principles based models and solving these by means of numerical codes in full toroidal geometry. These models are continuously being developed and benchmarked against existing codes at other associations. The dynamics of bursts of fluctuations leading to profile relaxation have been studied in models for flux-driven interchange mode turbulence, where the back reaction of the turbulence on the equilibrium flows and profiles are accounted for.
- *Fast Ion Collective Thomson Scattering.* Risø has taken the lead in the development of fast ion collective Thomson scattering diagnostics for TEXTOR, ASDEX upgrade (AUG) and ITER. These projects are carried out in close collaborations with MIT, and with the TEC[†] and AUG teams.

Fusion Technology, which includes:

- Experimental and theoretical investigations of the effects of irradiation on the microstructural evolution and on the physical and mechanical properties of metals and alloys relevant to the Next Step, the Long Term and Underlying Fusion Technology Programme.

The **global indicators** for the Research Unit in 2003 are:

• Professional staff	13.7	man-years
• Support staff	7.8	man-years
• Total expenditure - incl. mobility	3.01	MioEuro
• Total Euratom support	0.72	MioEuro

[†] TEC: the Trilateral Euregio Cluster, comprising Association EURATOM-Forschungszentrum Jülich GmbH, Institut für Plasmaphysik, Jülich, Germany; Association EURATOM-FOM, Institute for Plasma Physics, Rijnhuizen, The Netherlands; and Association EURATOM-ERM/KMS, Belgium.

2. Plasma physics and technology

2.1 Introduction

The year 2003 saw the activities in plasma physics and technology at Risø expand while activities in fluid dynamics were scaled back and pursued principally where direct synergy with efforts in plasma science exist. This shift in emphasis is reflected in the fact that with the New Year the programme, which is home to the bulk of Association EURATOM-Risø's activities, changes name from *Plasma and Fluid Dynamics* to *Plasma Physics and Technology*. As a follow-on from that, the department home changes name to *Optics and Plasma Research Department.* With this shift we concentrate and build on our core competence in plasma physics, spanning the field from the high temperature plasmas required for fusion energy to low temperature plasmas for a broad range of current and near term environmental and industrial applications. The latter include cleaning of exhaust gasses, sterilisation, material synthesis, and modification of surfaces for instance to improve adhesion.

A plasma is a dense collection of free ions and electrons. The transitions from solids to fluids to gases are associated with increases in internal energy, the breaking of bonds and changes of physical properties. The same is true of the transition from a gas to a plasma; in fact the plasma is rightfully described as the fourth state of matter, its physics differing as much from that of gases as that of solids does. Just as solid state physics is involved in a broad range of applications, so it should be no surprise that plasmas have a broad range of applications, that their physics and chemistries are rich, and that the methods of generation and diagnosis are wide and complex. Competences in plasma physics gained in pursuit of one goal form an excellent base for pursuing other applications involving plasmas.

Our activities in high temperature plasmas, aimed at developing fusion energy, are coordinated with the European EURATOM fusion programme through an agreement of association on equal footing with other fusion laboratories in Europe. Our EURATOM association facilitates extensive collaboration with other fusion research laboratories in Europe, crucial in the ongoing build-up of competences at Risø, and gives us access to placing our experimental equipment on large fusion facilities at the Max-Planck Institute for Plasma Physics in Garching and at the Research Centre Jülich, both in Germany. Our association with EURATOM also provides the basis for our participation in the exploitation of the European fusion research centre, JET, located in England. The European fusion programme, with its organisation of programmes at national laboratories as EURATOM associations, is a successful example of a large *European Research Area.* Our activities in high temperature plasma research and the development of fusion energy are introduced in subsection 2.2, and described in further detail in subsection 2.3 discussing turbulence and transport in fusion plasmas, and in subsection 2.4 discussing our use of millimetre waves for investigating the dynamics of fast ions in fusion plasmas.

2.2 Fusion plasma physics

Producing significant amounts of fusion energy requires a plasma with a temperature of 100 to 200 million degrees and densities of 1 to 2 times 10^{20} particles per cubic metre, corresponding to a pressure of 1 to 5 atmosphere. Plasmas, unlike gasses, can be confined and compressed by magnetic fields. At the required temperatures the plasma must be lifted off material walls to prevent the plasma from rapidly cooling. This is done by suspending the plasma in a toroidally shaped magnetic field which also acts to balance the plasma pressure.

The required temperature and densities have been achieved in the joint European fusion experiment, JET. The production of net energy adds the requirement that the energy in the plasma be confined at least on the order of 6 seconds. The confinement time is the characteristic time for cooling off if heating was switched off, or equivalently the ratio between plasma energy and required heating power to sustain that energy content. Achieved confinement times are on the order of 1 second. Higher density could compensate shorter confinement time and visa versa; so a simplified statement of the target is that the product of temperature, density and confinement time should be 6 atmosphere seconds and is currently 1 atmosphere seconds. Progress towards the goal principally involves improving the confinement time, or equivalently reducing the energy transport in the plasma. The energy transport in fusion grade plasmas is principally due to turbulence, one of our main research activities which is reported in subsection 2.3. Significant progress towards the goal is expected with the next step fusion experiment, ITER, which has been designed and currently is being negotiated between the participants, Europe, Japan, Russia, USA, China and Korea. In ITER significant fusion rates are expected and with that the fast ion populations in the plasma will dramatically increase compared with present machines. The fast ions may then significantly influence the plasma and is thus one of the central physics issues to be studied in ITER. It is in fact also one of our main research topics in fusion as reported in subsection 2.4.

The fields of turbulence, transport and fast ions are closely knit. With steep gradients in plasma equilibrium parameters and with populations of energetic ions far from thermal equilibrium, fusion plasmas have considerable free energy. This energy drives turbulence, which in turn acts back on the equilibrium profiles and on the dynamics of the fast ions. The turbulence naturally gives rise to enhanced transport, but also sets up zonal flows that tear the turbulent structures apart and give rise to edge transport barriers; most likely at the root of the poorly understood, but experimentally reliably achieved, high confinement mode (H-mode). This non-linear interplay between turbulence and equilibrium also supports transient events reminiscent of edge localized modes (ELMs) where energy and particles are ejected from the plasma edge in intermittent bursts.

This set of topics is the focus of our fusion plasma physics research: With first-principles based codes we seek to model the interplay between plasma turbulence, transport and equilibrium. This modelling is tested against experimental data in collaboration with other fusion plasma physics institutes. To elucidate the physics of fast ions and their interplay with turbulence, waves and transient events, we are engaged in the diagnosis of confined fast ions by collective Thomson scattering (CTS) at the TEXTOR tokamak at the Research Centre Jülich, Germany, and at the ASDEX upgrade tokamak in the Max-Planck Institute for Plasma Physics in Garching, Germany.

Our aim is not only to understand the dynamics, but also to identify external actuators with which the turbulence and transport can be controlled. The first demonstrations of edge turbulence control with arrays of electrostatic probes have been made in a linear device in collaboration with other associations. Selective ejection of core fast ions by sawteeth, which in turn can be manipulated by a localized heating and current drive, was found in fast ion CTS data obtained at TEXTOR in collaboration with TEC[1] and MIT, USA.

1. TEC: the Trilateral Euregio Cluster, comprising Association EURATOM-Forschungszentrum Jülich GmbH, Institut für Plasmaphysik, Jülich, Germany; Association EURATOM-FOM, Institute for Plasma Physics, Rijnhuizen, The Netherlands; and Association EURATOM-ERM/KMS, Belgium.

2.3 Turbulence and transport in fusion plasmas

O. E. Garcia, V. Naulin, A. H. Nielsen and J. Juul Rasmussen
volker.naulin@risoe.dk;
jens.juul.rasmussen@risoe.dk

The transport of heat and particles across the confining magnetic field of fusion plasmas is one of the most important and interesting, but also difficult areas of contemporary fusion research. It is well established that the "anomalous" transport component mediated by low frequency turbulence is far larger than the classical collisional transport. It is thus of utmost importance to achieve a detailed understanding of this transport and the underlying turbulence for the design of an economical advanced fusion reactor based on magnetic confinement schemes. In spite of a dramatic progress in experiment, theory and computations during recent years the quantitative understanding is still very sparse and any predictive capacity is at best rudimentary. Even very fundamental phenomena such as transitions from low confinement regime (L-mode) to high confinement regime (H-mode), the profile resilience and the particle pinch that are routinely observed and classified experimentally have no generally accepted explanations.

We have mainly focussed our activities in plasma turbulence and transport on topics related to edge turbulence. It is found that the conditions near the edge of the plasma are dictating the global performance, which seems natural since all transport has to go through the edge region. Our investigations are based on numerical solutions of first principle models, and we aim at benchmarking results and performance with other codes and also with experimental observations when available.

Our investigations have comprised direct numerical simulations of both impurities and tritium transport in the edge plasma region (see 2.3.1), where we found strong asymmetric transport features with a dominating pinch convection on the low-field side and an anti-pinch, i.e., outward convection, at the high-field side. In the contributions 2.3.2-2.3.3 we consider the bursting and intermittency in the fluxes of particles and heat, which come about due to nonlinear energy exchange between global poloidal flows and small scale turbulent fluctuations. It is notable that in contribution 2.3.2 we have derived a new energy conserving global model for transport at the transition from the edge to the scrape-off-layer (SOL). Results from this model reproduce in detail recent experimental observations of plasma blobs propagating far out into the SOL. These propagating blobs are responsible for strongly intermittent bursts of hot plasma, which pose a problem to plasma facing components in next step devices.

In general, the turbulence and transport in fusion devices is observed to be strongly intermittent. In 2.3.4 we describe experimental investigations of the intermittency of small-scale fluctuations in Wendelstein 7-AS during controlled transitions in the confinement. The investigations are based on collective scattering measurements of density fluctuations utilizing the equipment constructed and run by Risø. The results indicate that the characteristics of the fluctuations are independent of the path to good or bad confinement.

In the plasma edge region the turbulent transport is found to be dominated by energetic bursts. Thus, the probability distribution functions (PDFs) of the particle and heat fluxes are skewed with fat tails, and are strongly deviating from Gaussian distributions. The mean value and variance of the PDF is therefore not sufficient to make predictions about the transport and the associated heat load on plasma facing components. It is essential to have knowledge of the full PDF, or at least higher order moments. In 2.3.5 we show that the transport PDF for a number of different models have similar structure; that is the tail of the PDFs are well described by an extreme value distribution and are consequently decaying exponentially and

not as a power law, as frequently speculated elsewhere. These results are utilized in collaboration with the Innsbruck Experimental Plasma Physics Group on the evaluation of fluctuation data from emissive probe measurements. The initial phase of this collaboration is described in 2.3.6.

The final topic is concerned with the generation of global shear flows by the turbulence, and the interplay between these flows and the turbulence and transport. These flows are assumed to play a crucial role in the transition from the low confinement to the high confinement regime (LH-transition). The importance of the self generation of these flows by the turbulence has become increasingly clear. However, the exact mechanisms are not yet quantitatively assessed. We have investigated the generic flow generation in drift-Alfvén turbulence in 2.3.7. For increasing plasma beta the so-called Maxwell stress will compete with the Reynolds stress and limit the flow generation, however, an additional effect due to the geodesic part of the curvature comes into play and adds to the shear flow. In 2.3.8 we consider a simple model of drift waves and investigate the parametric dependence of the width of zonal flow bands. Finally, in 2.3.9 we report on our investigations of the linear instability features of interchange modes in the presence of imposed shear flows of various profiles.

2.3.1 Impurity and trace tritium transport in tokamak edge turbulence

V. Naulin (work performed while seconded to JET under the EFDA agreement)
volker.naulin@risoe.dk

The transport properties of impurities are of great concern in magnetic fusion devices. Pinching of impurities has been observed as well as fast inward transport of trace Tritium in JET Tritium puffs. We here investigate the transport of passive impurity species in electromagnetic edge plasma turbulence. The turbulence is generated by a fluctuation model in flux-tube geometry and for the passive species we consider cold ions of finite mass.

Impurities released at the high field side experience an anti-pinch, and while diffusing are convected out of the plasma, while particles released on the low field side are sucked into the plasma by a pinch effect, see Figure 1.

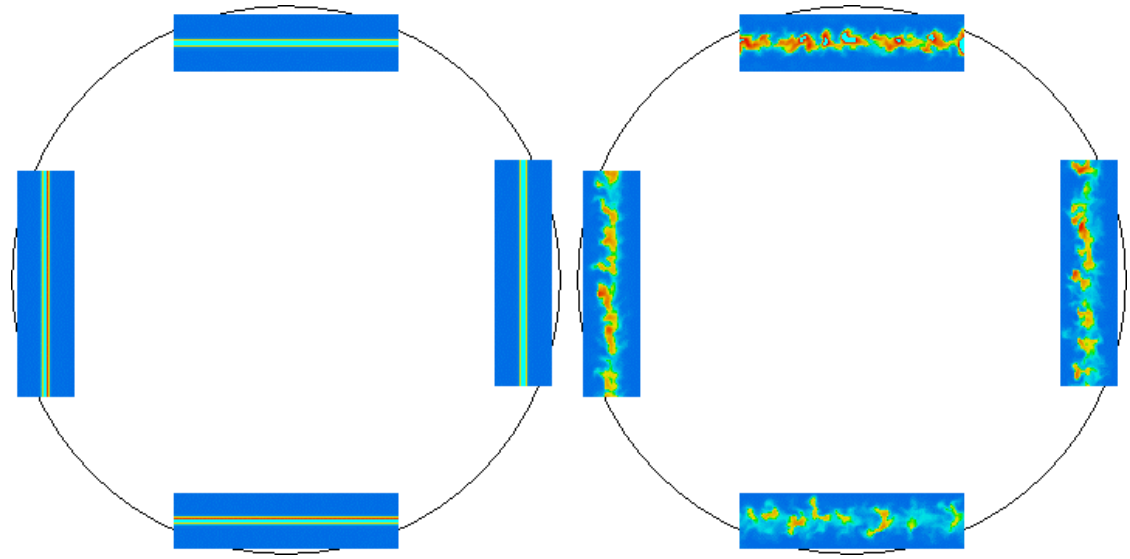

Figure 1. Impurity density in edge turbulence. Left initial distribution, right after 50 micro seconds. A poloidally varying pinch effect is seen.

Initial investigations show very reasonable agreement with experiments and demonstrate that impurity transport needs at least a two-dimensional transport model resolving both radial and poloidal coordinates. This initial investigation also showed that the description of the transport Γ as given by a diffusion value D and a pinch velocity V can be justified as a first approximation.

2.3.2 Intermittent transport in scrape-off layer plasmas

O. E. Garcia, V. Naulin, A. H. Nielsen and J. Juul Rasmussen
odd.erik.garcia@risoe.dk

The radial transport of plasma and heat is universally observed to be highly intermittent in the scrape-off layer (SOL) of magnetic plasma confinement experiments. From local probe measurements it is generally observed in magnetized plasmas that the averaged density, temperature and electric field signals possess asymmetric waveforms with a sharp rise and slow decay, similar to the waveform from our numerical results depicted in Figure 2. Moreover, the probability distribution functions (PDFs) are positively skewed and flattened, indicating propagation of thermal structures through the SOL region. Theoretical and computational descriptions of SOL turbulence have so far assumed a local generation of turbulent fluctuations due to steep pressure gradients in the SOL region. However, experimental measurements reveal a flattened pressure profile throughout the SOL. This indicates that the observed waveforms may be due to blobs of plasma and heat ejected from the core or edge plasma and travelling through the SOL region, assuming the blob transition time through the SOL is short compared with the measurement integration time.

A new model for non-linear interchange modes has been derived which yields a conservative energy transfer between kinetic energy due to E×B drifts and thermal energy.[1] This model emphasizes the non-linear collective dynamics while a simplification is made for the dissipative processes due to particle losses along open magnetic field lines in the SOL. Forcing is invoked by means of a heat source in the edge region with closed field lines, but magnetic shear has been neglected to allow a two-dimensional description. Long-run numerical solutions of this model covering the longest time scales reveal a regulation process due to self-sustained sheared flows, resulting in bursting in the fluctuation level in the edge region and relaxation oscillations in the confined heat and the total mean flow energy. The repetitive generation of sheared flows by fluctuating motions leads to ‘‘flapping’’ of the edge pressure gradient ejecting blobs of hot plasma into the SOL. Also the statistical properties of the propagating structures are in excellent agreement with experimental observations. In particular, we observe asymmetric waveforms, positively skewed and flattened PDFs, and radial propagation velocities up to one tenth of the sound speed. In Figure 2 we show the conditionally averaged density signal, using the trigger condition $n > 4n_{rms}$, and the PDF of the density signal at different radial positions. The highly intermittent transport events sets the heat load that the plasma facing components in next generation confinement experiments must withstand.

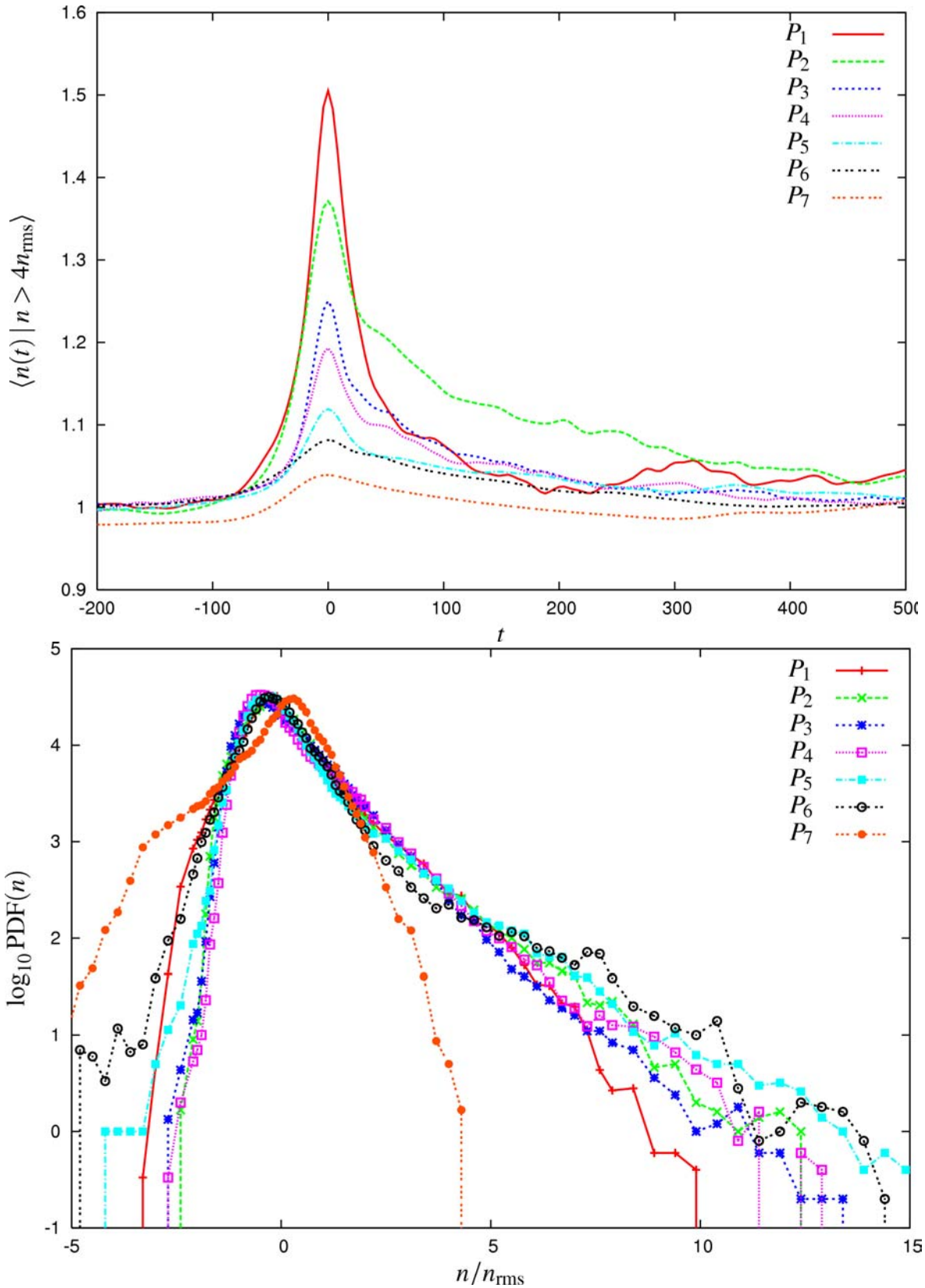

Figure 2. Results of the long time numerical simulations: Upper panel: Conditionally averaged density signals as measured at 7 different radial positions. P1 is inside last closed flux surface and P7 is in the far SOL. Lower panel: The probability distribution functions of the density fluctuations measured at the same positions.

1. O. E. Garcia, V. Naulin, A. H. Nielsen, and J. Juul Rasmussen, ‘‘Intermittent transport in scrape-off layer plasmas’’, http://arxiv.org/abs/physics/0309020.

2.3.3 Self-regulation, bursting and large-scale intermittency in convective turbulence

O. E. Garcia and N. H. Bian (Istituto Nazionale Fisica della Materia, Department of Energetics, Politecnico di Torino, Italy)
odd.erik.garcia@risoe.dk

Rotating fluids and magnetically confined plasmas are prone to quasi-two-dimensional fluctuations leading to substantial radial transport of particles and heat. The fluctuating motions may undergo a secondary instability leading to the formation of differential rotation in the azimuthal directions, which can strongly reduce the non-linear transport and thus improve the heat confinement. Examples include thermonuclear fusion experiments and atmospheres of rotating planets.[1-3] Commonly observed in such systems are low frequency bursting in the fluctuation level and relaxation oscillations in the mean flow energy level as well as in the heat confinement when the latter is allowed to vary.

The net turbulent transport thus appears as quasi-periodic bursts separated by quiet phases. The prevailing theory for such a self-regulating behaviour is based on the shearing effect due to differential advection by the mean azimuthal flows. This shearing is essentially a spectral expulsion of fluctuation energy to large radial wave numbers, leading to enhanced dissipation of convective structures and hence less turbulent transport.

The work reported here has demonstrated that an alternative interpretation may be given simply in terms of the energy conserving interaction between fluctuating and mean flows.[1-3] This interpretation readily explains the formation of improved confinement regimes due to sheared flows, observed in experiments and computer simulations. This point of view emphasizes the intrinsic dynamical nature of convective systems and precludes the wide-spread interpretation in terms of linear stabilization of convective modes by sheared flows. A variety of computations demonstrate the essential role of energetics for transport regulation by self-sustained sheared flows.[1,2] The bursting regime has further been demonstrated by phenomenological predator-prey-like models, also showing that the collisional dissipation of the mean profiles determines the time scale for the low frequency relaxation oscillations.[2,3]

Another regulation mechanism resulting in transport bursting is shown to result from the quasi-linear modification of the pressure profile from the turbulent heat transport.[3] The frozen-profile approximation, frequently applied in massive computations, rules out this important effect. For both regulation mechanisms, numerical simulations have demonstrated that the low frequency bursting gives rise to large-scale intermittency, manifested by exponential tails in the probability distribution functions of single-point recording of the fluctuating fields.[1,2] Moreover, this leads to high spectral energy content at low frequencies, which is frequently confused with self-organized critical behaviour.

1. O. E. Garcia, N. H. Bian, J.-V. Paulsen, S. Benkadda, and K. Rypdal, ‘‘Confinement and bursty transport in a flux-driven convection model with sheared flows’’, *Plasma Phys. Control. Fusion* **45**, 919 (2003).
2. O. E. Garcia and N. H. Bian, ‘‘Bursting and large-scale intermittency in turbulent convection with differential rotation’’, *Phys. Rev.* E **68,** 047301 (2003).
3. N. H. Bian and O. E. Garcia, ‘‘Confinement and dynamical regulation in two-dimensional convective turbulence’’, *Phys. Plasmas* **10**, 4696 (2003).

2.3.4 Study of intermittent small-scale turbulence in Wendelstein 7-AS plasmas during controlled confinement transitions.

N.P. Basse (Plasma Science and Fusion Center, Massachusetts Institute of Technology, MA, USA), S. Zoletnik (CAT-Science, Budapest, Hungary), P.K. Michelsen, W7-AS Team, (IPP, Garching, Germany)
poul.michelsen@risoe.dk

The role of plasma turbulence in confinement transitions, both induced and spontaneous, is currently being investigated in most magnetic confinement fusion devices. This work is part of that continual effort, and focuses on internally and externally induced confinement transitions.

It is a well known fact that confinement in the Wendelstein 7-AS (W7-AS) stellarator[1] is very sensitive to the boundary value of the rotational transform, ι_a. Here, a is the minor radius of the plasma. Optimum confinement is found in narrow ι_a-windows close to (but not at) low-order rationals $\iota_a = 1/2, 1/3$ etc. The special significance of these windows is that they are free from the otherwise densely spaced higher-order rational ι_a-values. Therefore it has been assumed that perturbations arising at higher-order rational surfaces enhance the electron transport. These perturbations could be either static (due to the magnetic field) or dynamic (due to turbulence or magneto-hydrodynamic activity). We are investigating the changes in electron density fluctuations associated with the varying confinement quality at different ι_a.

The diagnostics available for our analysis are Mirnov coil measurements of magnetic fluctuations and the collective scattering measurements of density fluctuations using an infrared light source, constructed and operated by Risø till the closure of W7-AS.

We have analysed discharge types in plasmas with edge rotational transforms ι_a close to 1/3, where confinement is very sensitive to small changes in ι_a. Good (bad) stationary confinement is achieved at $\iota_a \sim 0.34$ (0.36) with zero net plasma current, and the transient good to bad confinement transition is obtained by having the external $\iota_a \sim 0.34$, while ramping up the net plasma current from zero to raise the total ι_a.

Our analysis has shown that the major spectral characteristics of the density fluctuations are independent of the path to good or bad confinement. This includes auto- and cross-power spectra and the speed of the density fluctuations. However, auto-power spectra of magnetic fluctuations display differences between transient and stationary discharges.

Correlation calculations between band auto-powers in the two density fluctuation measurements volumes showed that the correlation increases for both the stationary and transient good to bad confinement transition. The density fluctuation power is intermittent, and the bursts are correlated between the bottom and the top of the plasma. Correlations between magnetic and density fluctuations confirmed the analysis performed using only density fluctuation measurements. The correlation time of the bursts is of order 100 μs, similar to the lifetime observed during edge localized modes. It is possible that the correlated fluctuations are due to large-scale zonal flows; that is a topic for future works.

1. H. Renner et al., *Plasma Phys. Control. Fusion,* **31,** 1579 (1989).

2.3.5 Statistical properties of transport in plasma turbulence

V. Naulin, O. E. Garcia, A. H. Nielsen and J. Juul Rasmussen
volker.naulin@risoe.dk

In hot magnetized plasmas the cross-field transport of particles and heat is mainly mediated by low frequency turbulence and is far larger than that expected from collisional diffusive transport. Additionally, the transport near the plasma edge is generally observed to be strongly

intermittent and dominated by strong bursts. Thus, the probability distribution functions (PDFs) of the particle and heat fluxes are skewed with fat tails and are strongly deviating from Gaussian distributions. The mean value and variance of the PDF is therefore not sufficient to make predictions of the transport and of the associated heat load on plasma facing components. It is essential to have knowledge of the full PDF, or at least higher order moments.

We have investigated the statistical properties of the turbulent particle flux in different types of plasma turbulence models. These models are solved numerically and the particle flux is characterized by the PDF. The physics included in the applied models range from two-dimensional drift wave turbulence to three-dimensional MHD dynamics. We have considered local fluctuation type models, based on a separation of the scale length of the background pressure gradient and the fluctuations as well as global models without scale separations and accounting for the full evolution of the background. The aim is to address the essential question on how the transport PDF depends on the driving mechanism behind the turbulence, and ultimately: will it be possible to devise a generic transport PDF that is governed by few parameters?

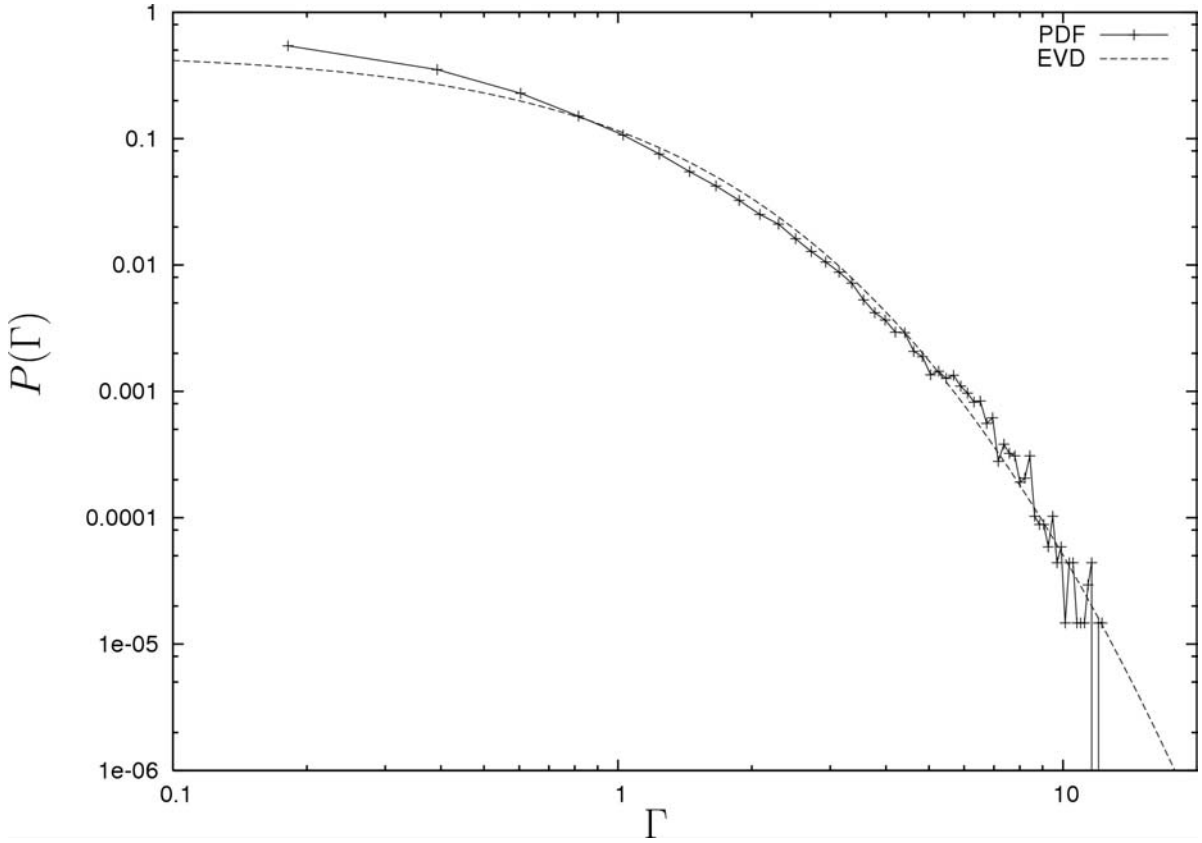

Figure 3. Tail of the flux-surface averaged particle transport fitted with an EVD for the global interchange model.

The PDFs of the flux measured at one point, which mimics the experimental measurements of the flux by probe arrays (see 2.3.6), show a strongly skewed PDF with a tail toward positive (outward) flux events. For the local models, where the PDF of potential and density fluctuations are close to Gaussians, the flux PDF is well described by a PDF of a random variable that result from the product of two correlated Gaussian distributed random variables[1]. Both for the global and local models the tails of the PDF are decaying exponentially and not as a power law, as frequently speculated elsewhere.

We also investigated the flux-surface averaged flux, and again the PDFs were skewed with a fat tail towards positive events. For the local models these PDFs are generally in good agreement with extreme value distributions (EVDs), implying that the tail decays exponentially. This may be interpreted as a signature of strong vortical structures dominating the transport on individual flux-surfaces. The global models exhibit properties distinctly different from those observed in the local models. Specifically, the flux-surface averaged particle fluxes from the former models have a sharp peak at low transport values. This is due to the bursting of the global fluctuation level (see, e.g., 2.3.2 and 2.3.3). The bursty behaviour is caused by a regulation mechanism due to self-sustained sheared mean flows. However, also for these global models the tails of the PDFs are well fitted to EVDs as seen in Figure 3.

1. B.A. Carreras, C. Hidalgo, E. Sánchez, M. Pedrosa, R. Balbín, L. García-Cortés, B. van Milligen, D.E. Newman, V.E. Lynch, *Phys. Plasmas* **3**, 2664 (1996).

2.3.6 Evaluation of measured turbulent particle fluxes in toroidal devices

P.C. Balan, R.W. Schrittwieser*, C. Ionita* (*Institute for Ion Physics, University of Innsbruck, Austria), O. E. Garcia, V. Naulin, A. H. Nielsen and J. Juul Rasmussen*
jens.juul.rasmussen@risoe.dk

Collaboration has been established between the Innsbruck Experimental Plasma Physics Group at the University of Innsbruck and Risø. The aim is to contribute to the evaluation of measurements of potential and density fluctuations, and of fluctuation driven particle flux and Reynolds stress performed by the Innsbruck group. The measurements are carried out by using arrays of emissive probes. Comparison of the measurements with results obtained from simulations of plasma turbulence is an important element in this collaboration. In the initial phase, we have mainly considered the evaluation of the particle flux, which can be obtained directly from measurements of the density fluctuations and the fluctuations in the radial velocity component (proportional to the poloidal electric field). It is generally found that single point measurements of the particle flux show strong non-Gaussian features, revealing probability distribution functions (PDFs), with a strong tail towards positive (outward) flux events. This is in agreement with results obtained in simulations (see 2.3.5) and expected for Gaussian density and electric field fluctuations. In order to obtain a quantity that may be compared with the flux-surface-averaged particle flux (see 2.3.5), we average the flux signal, measured at a single position, over some time interval comparable to the correlation time, to create a new series of random variables consisting of these "short-time" averaged fluxes. The underlying assumption is that the fluctuations are propagating mainly in the poloidal direction. The PDF of this quantity is found to be well described by the extreme value distribution as was found for the flux-surface averaged flux in the simulations (see 2.3.5), although more data and in particular longer experimental time series will be needed for a detailed comparison.

2.3.7 Shear flow generation in electromagnetic plasma edge turbulence

V. Naulin, O. E. Garcia, A. H. Nielsen, J. Juul Rasmussen and A. Kendl
volker.naulin@risoe.dk

Shear flows play a crucial role in the transition from the low confinement to the high confinement regime in magnetically confined fusion plasmas (LH transition). The importance of turbulence as an ingredient to their formation has over the last years become increasingly clear. The exact way the small-scale turbulence is able to set up flows and by this to interact with the meso-scale is, however, not yet completely understood and a self-consistent model of the LH transition is consequently lacking.

The flow generation in turbulence is due to a number of different mechanisms, the most well known being the Reynolds stress, describing the momentum transport by the turbulence. In electromagnetic turbulence the Reynolds stress is accompanied by the Maxwell stress, reflecting the momentum transport along perturbed magnetic field lines. To complicate the situation for complex magnetic field geometry a third contribution arises from the geodesic part of the curvature.

The relative importance of these three mechanisms is investigated for drift-Alfven turbulence by following the detailed energy transfers into the flow component. Initial results indicate that for higher plasma beta the Reynolds stress is dwarfed by the Maxwell stress. Furthermore, the geodesic curvature results in a transfer of energy into the flow component for large values of the plasma beta. In Figure 4 we show the energy input into the flow from the Reynolds and Maxwell stresses and from the geodesic acoustic modes.

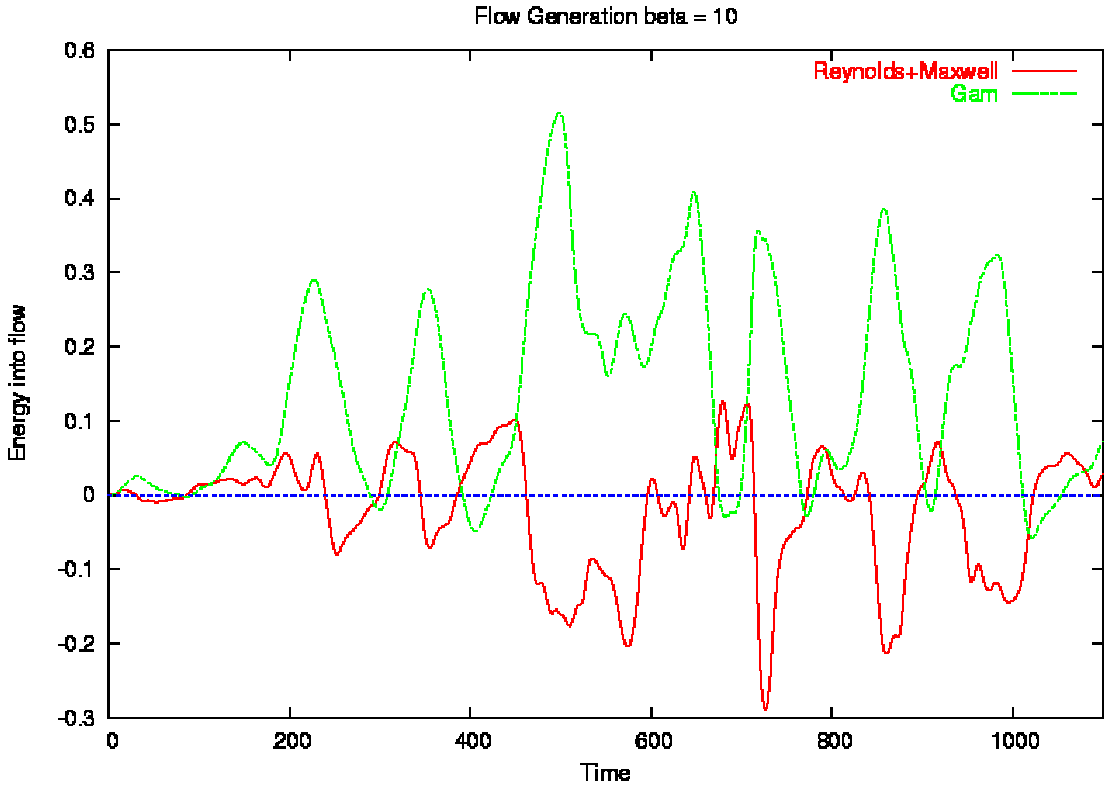

Figure 4. Energy input into the flow from the Reynolds and Maxwell stresses and from the geodesic acoustic modes (GAMs).

2.3.8 Numerical investigations of large-scale zonal flows in drift wave turbulence

A.H. Nielsen, S. Delaux (MATMECA, Université Bordeaux, France), V. Naulin, O.E. Garcia and J. Juul Rasmussen
anders.h.nielsen@risoe.dk

The self-consistent generation of large-scale flows by the rectification of small-scale turbulent fluctuations is of great importance both in magnetically confined plasmas and in geophysical flows[1,2]. These flows regulate the turbulence suppressing the small-scale structures and set-up transport barriers.

We have modelled the generation of zonal flows by drift wave turbulence in magnetized plasma as described by the Hasegawa-Mima-Charney equation on a cylinder:

$$\frac{\partial}{\partial t}\left(\nabla^2\phi-\phi\right)+\frac{1}{r}\left[\phi,\nabla^2\phi\right]-\beta\frac{1}{r}\frac{\partial\phi}{\partial\theta}=\nu\Delta^2\phi-\eta\Delta\phi+F(\vec{r})\sin(\gamma t),$$

where ν is the kinematic viscosity and η a sheath damping. The last term in the equation is a body forcing term, where $F(\vec{r})$ is an array of vortices with opposing signs, illustrated in the first frame in Figure 5.

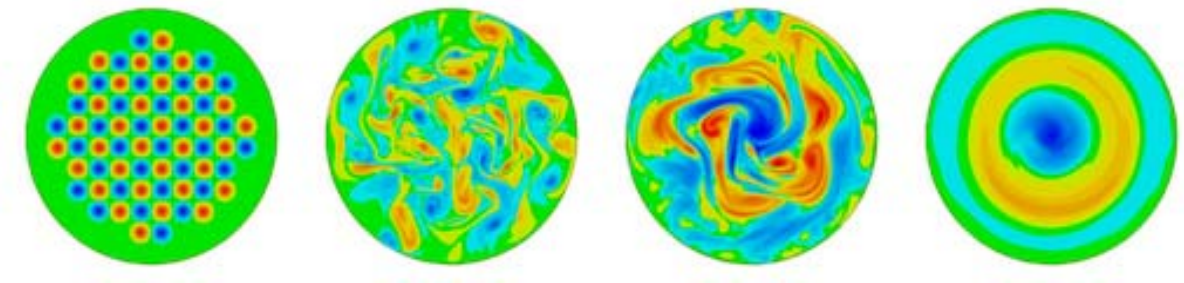

Figure 5. Temporal evolution of the electric potential, ϕ, for t=0, t=100, t=500 and t=1000. Parameters: ν=0.00001, β=0.256 and η=0.

We have numerical integrated the differential equation for different values of β on a disk applying stress-free boundary condition[3]. In Figure 5 we display the temporal evolution of the electric potential, ϕ, where we have used an array of vortices as initial condition. After a turbulent phase, where larger structures are created by vortex-vortex merging, the flow settles into a regular pattern consisting of bands of potentials with opposing signs. For increasing values of β we generally observe more, but weaker bands.

1. P.W. Terry, *Rev. Mod. Phys.* **72**, 109 (2000).
2. P.B. Rhines, *Ann. Rev. Fluid Mech.* **11**, 401 (1979).
3. V. Naulin et al, *AIP Conf. Proc*. **669**, 662 (2003).

2.3.9 Do sheared flows inhibit interchange instability?

E.S. Benilov (Dept. Mathematics, University of Limerick, Ireland),
V. Naulin and J. Juul Rasmussen
jens.juul.rasmussen@risoe.dk

The suppression of turbulence and thereby of the associated transport by externally imposed or self-generated poloidal ExB-shear flows seems by now to be so widespread in the plasma context that it is believed to be universal[1]. This is in contrast to the general consensus in the hydrodynamics community, where it is well established that shear flows (with a finite curvature of the flow velocity profile) are generally unstable and that added shear flows act destabilizing rather than stabilizing, although there are examples of stabilizing effects in nonionized flows in particular in geophysical flows.

To contribute to this standing discussion we have examined the particular example of shear flow effects on the interchange instability, which is unavoidable in a plasma with curved magnetic field lines. The investigations are performed by direct solutions of the eigen-problem for the linear instability on a bounded domain modeling the edge region in a toroidal plasma. We examined the stability properties for several shear flow profiles. Generalizing the obtained results, we draw the following conclusions:

The stabilizing effect of variable shear is much weaker than that of the uniform one. Flows with sufficiently large shear anomaly cannot be stabilized no matter how strong the mean shear is.

Flows in a large slab are, generally, more unstable than those in a small one. There are strong indications that, in the absence of walls, flows with variable shear are all unstable - no

matter how strong the mean shear is, and how weak the shear anomaly is. All examples of flows with non-monotonic profiles turned out to be unstable.

Overall, given that realistic plasma flows always have variable shear, they appear to be unable to eliminate interchange instability (although they can still weaken it). We should, however, note that, in all examples considered, the instability had a short-wave cutoff, i.e., disturbances with $k>k_0$ are stable. Hence, if the poloidal length, L_y, is such that $L_y<2\pi/k_0$ the flow should become stable. However, to explore this possibility in detail one should examine a full toroidal problem.

1. P. W. Terry, "Suppression of turbulence and transport by sheared flow", *Rev. Mod. Phys*. 72, 109 (2000).

2.4 Millimetre waves used for diagnosing fast ions in fusion plasmas

H. Bindslev, S.B. Korsholm, F. Meo, P.K. Michelsen, S. Michelsen, S.K. Nielsen and E.L. Tsakadze
henrik.bindslev@risoe.dk
www.risoe.dk/euratom/cts

Millimetre waves, corresponding to frequencies in the 100 GHz range, permit probing and imaging on the centimetre scale and transmission of signals with bandwidths in excess of 10 GHz. Coherent sources are now available from the micro- to Megawatt range, CW. These technologies, widely used in fusion research, and in many cases specifically developed for fusion research, are now being considered for a broader range of commercial applications. These include new GigaBit wireless internet highways and wide area networks which avoid expensive trenching of optical fibres.

In the world of fusion, the millimetre waves are used extensively both as a diagnostic tool and as an actuator for manipulating the plasma locally as well as globally. Central to achieving these objectives is the fact that millimetre waves, like laser light, can be projected in narrow focused beams and, unlike laser light, the millimetre waves can interact strongly with the plasma.

At Risø we are developing millimetre wave diagnostics for measuring the velocity distribution of the most energetic ions in fusion plasmas. The measurements will be resolved in space on the centimetre scale and in time on the millisecond scale.

The most energetic (or fast) ions are the result of fusion reactions and auxiliary heating. Their interaction with the bulk plasma is the main mechanism by which the fusion plasmas reach and sustain the high temperatures of 100-200 million degrees Kelvin, required for fusion. The considerable energy associated with the fast ions can also drive turbulence in the plasma, and degrade the confinement of the plasma and of the fast ions themselves. Understanding and controlling the dynamics of fast ions are central tasks in the development of fusion energy, and one of the main research topics for the next large fusion facility, ITER. It is a task we seek to tackle by developing and exploiting the unique diagnostic capability of millimetre wave based collective Thomson scattering (CTS).

The group is currently developing fast ion CTS diagnostics for the TEXTOR and ASDEX-Upgrade tokamaks, which are located at the Research Centre Jülich in Germany and at the Max-Planck Institute for Plasma Physics in Garching, also in Germany. Further details of this work are given in subsections 2.4.1 and 2.4.2.

Construction and pre-installation testing of the ASDEX CTS system was completed and the system was installed in Garching in December 2003. The system for TEXTOR is under

construction and testing at Risø. These projects are conducted in collaboration with MIT, the Max-Planck Institute for Plasma Physics in Garching and the TEC[1] consortium.

The CTS efforts at Risø in 2003 included a study of the feasibility of measuring the fast ion phase space distribution in ITER by CTS, described in further detail in subsection 2.4.6. The study covers the full range of potential probe frequencies from gyrotron based millimetre waves to the infrared light of the CO_2 laser. It was assessed whether the systems can meet the ITER measurement requirements and which technological developments may be required. The relative merits of the systems were compared. The study reveals that a CTS system based on a 60 GHz probe has the highest diagnostic potential, and is the only system expected to be able to meet all the ITER fast ion measurement requirements with existing or near term technology. A conceptual design was developed and costs estimated, details of which are given in subsection 2.4.7. With modest additions this system may also provide measurements of the fuel ion ratio.

On the basis of the millimetre wave activities for diagnosing fusion plasmas, the group responded to a call for solutions for private wireless AV transmission for music festivals and other venues. A system, using 94 GHz mm waves, was successfully demonstrated.

"Implementation of Fast Ion Millimeter Wave CTS Diagnostics on TEXTOR and ASDEX Upgrade", S. B. Korsholm, H. Bindslev, J. Egedal, J. A. Hoekzema, F. Leuterer, F. Meo, P. K. Michelsen, S. Michelsen, E. L. Tsakadze and P. Woskov, *45th Annual Meeting of the Division of Plasma Physics, American Physical Society* (DPP-APS), Albuquerque, New Mexico, October 27 – 31, USA, 2003.

"Fast Ion Millimeter Wave CTS Diagnostics on TEXTOR and ASDEX Upgrade", S. B. Korsholm, H. Bindslev, J. Egedal, J. A. Hoekzema, F. Leuterer, F. Meo, P. K. Michelsen, E. Tsakadze and P. Woskov, *30th EPS Conference on Controlled Fusion and Plasma Physics*, St Petersburg, Russia, July 7-11, 2003.

"Fast ion millimeter wave CTS diagnostics on TEXTOR and ASDEX", S. B. Korsholm, H. Bindslev, J. Egedal, J. A. Hoekzema, F. Leuterer, P. K. Michelsen, E. Tsakadze, and P. Woskov, *44th Annual Meeting of the Division of Plasma Physics, American Physical Society* (DPP-APS), Orlando, Florida, USA (2002). Bulletin of American Physical Society (APS), p. 84, vol. 47, N 9, November, 2002.

2.4.1 Construction of the collective Thomson scattering diagnostic upgrade for TEXTOR

S. B. Korsholm (also at MIT Plasma Science and Fusion Center, Massachusetts, USA), H. Bindslev, J. Egedal, J. A. Hoekzema (Association EURATOM-Forschungszentrum Jülich GmbH, Institut für Plasmaphysik, Jülich, Germany), F. Meo, P. K. Michelsen, S. Michelsen, E. L. Tsakadze, and P. Woskov* (*MIT Plasma Science and Fusion Center, Massachusetts, USA)*
soeren.korsholm@risoe.dk
www.risoe.dk/euratom/cts/textor

In 2000-2001 the pilot version of the CTS system at TEXTOR, a collaborative effort between FOM, Netherlands and MIT, USA, obtained many useful data using a 100 kW, 0.2 s, 110 GHz gyrotron. However, due to the location of the CTS electronics close to the tokamak and configuration changes on TEXTOR itself, noise became an increasing problem. Furthermore, an upgrade of the antenna and receiver electronics was desirable, and a new data acquisition system was required.

[1] TEC: the Trilateral Euregio Cluster, comprising Association EURATOM-Forschungszentrum Jülich GmbH, Institut für Plasmaphysik, Jülich, Germany; Association EURATOM-FOM, Institute for Plasma Physics, Rijnhuizen, The Netherlands; and Association EURATOM-ERM/KMS, Belgium.

In 2002 and 2003 a new quasi-optical transmission line was designed and constructed at Risø. The work on the transmission line is described in more detail in subsection 2.4.3. The main advances are a steerable (±30°) quasi-optical antenna mirror, a universal polarizer and that the quasi optical transmission line permits locating the electronics far (3-4 m) from the tokamak (See Figure 6).

The receiver electronics has also been upgraded and a new data acquisition system constructed with 40 channels sampled at 100 kHz with 24-bit resolution. The data acquisition system will allow complete coverage of the double sideband scattered spectrum for localised (<10 cm), time resolved (~4 ms) ion velocity distribution measurements corresponding to an ion deuterium energy range of approximately 0.5 to 200 keV.

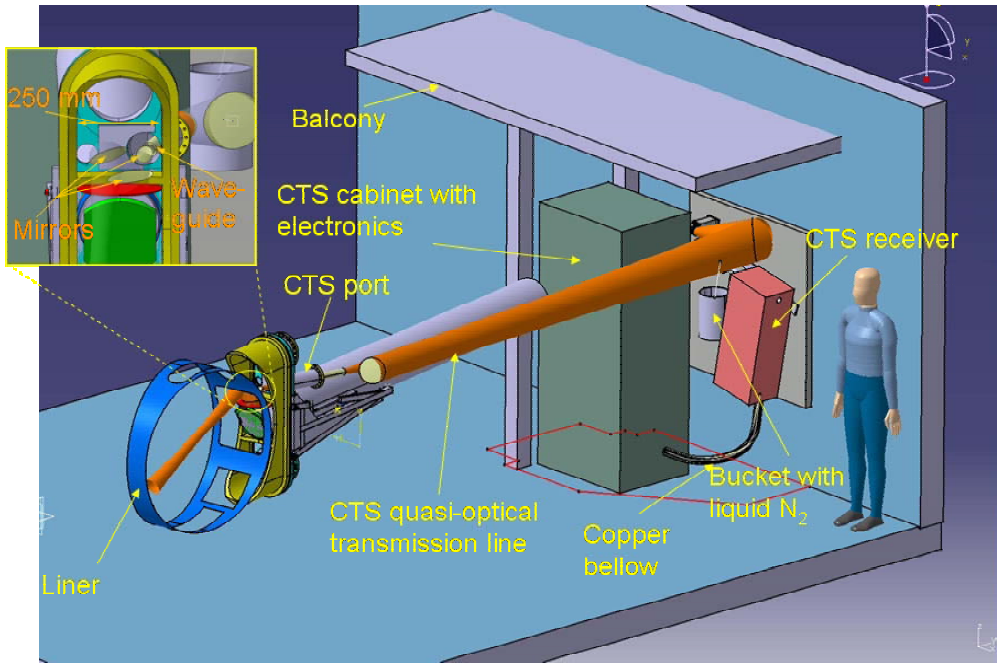

Figure 6. Overview of the TEXTOR CTS system. The quasi-optical beam is shown in orange.

Installation of the diagnostic is scheduled for the beginning of March 2004, with operation and full system tests (including the 110 GHz gyrotron) commencing in May 2004.

2.4.2 Construction and installation of the collective Thomson scattering diagnostic at ASDEX Upgrade

S. B. Korsholm (also at MIT Plasma Science and Fusion Center, Massachusetts, USA), H. Bindslev, J. Egedal, F. Leuterer (Max-Planck-Institut für Plasmaphysik, EURATOM Association, Garching, Germany), F. Meo, P. K. Michelsen, S. Michelsen, E. L. Tsakadze, and P. Woskov* (*MIT Plasma Science and Fusion Center, Massachusetts, USA)*
soeren.korsholm@risoe.dk
www.risoe.dk/euratom/cts/aug

Besides the upgrade of the existing TEXTOR CTS system (described in subsection 2.4.1), a new system has been designed, built and installed at ASDEX Upgrade at the Max-Planck Institute for Plasma Physics in Garching, Germany.

A major upgrade of the ASDEX Upgrade ECRH system is currently under way. It will contain four gyrotrons of 1 MW each, operating at 105 GHz and 140 GHz. This will bring the total heating power of ASDEX Upgrade above 30 MW (incl. more than 20 MW ion heating). The substantial ion heating produces large populations of fast ions.

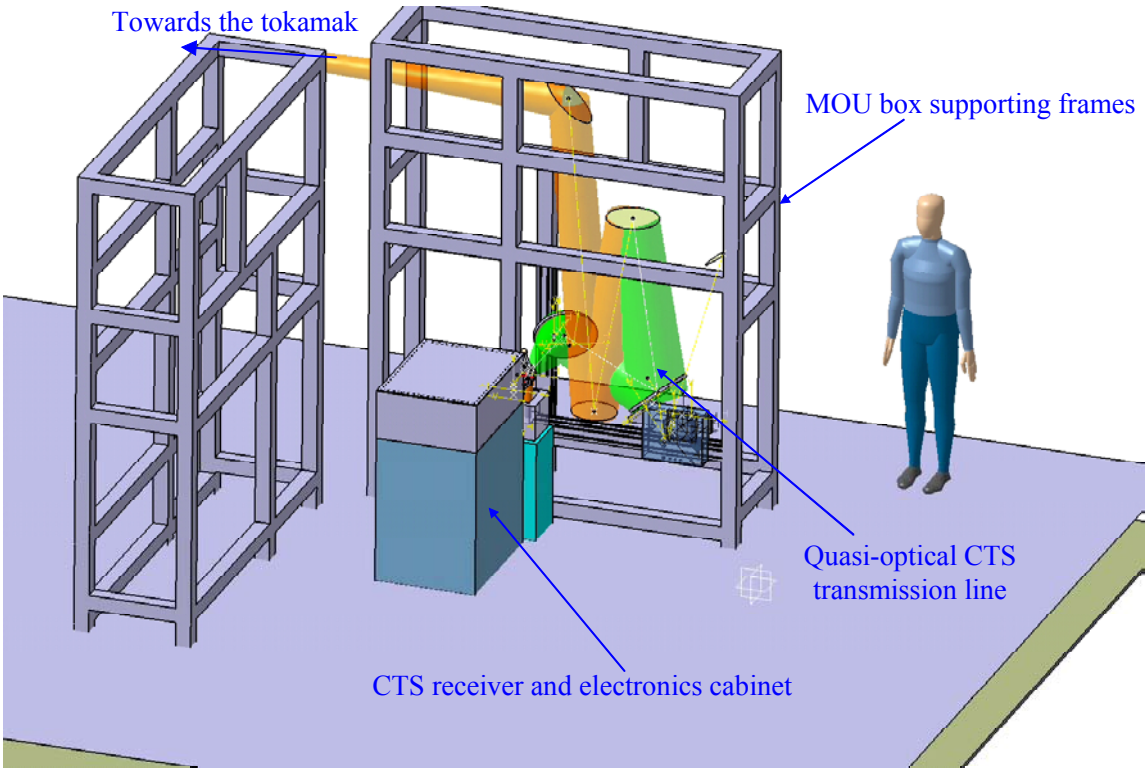

Figure 7. Overview of the CTS diagnostic for ASDEX Upgrade.

Figure 8. The CTS diagnostic for ASDEX Upgrade after installation, December 2003.

The ASDEX Upgrade CTS diagnostic will use the new ECRH system, in particular the new dual frequency gyrotron (105 GHz, 1 MW, 10 sec pulse length) and the transmission lines. One of the quasi-optical transmission lines from the vessel to the gyrotron will be modified for the optional use of the CTS antenna or the gyrotron. The design of the transmission line modification is further described in subsection 2.4.3, while an outline sketch of the system is presented in Figure 7.

The ASDEX Upgrade CTS system was installed in early December 2003 (see Figure 8). The time schedule for the exploitation of the diagnostic is dependent on the installation of the gyrotron and the relevant parts of the ECRH system. It is expected that operation of the system will commence in the summer of 2004.

2.4.3 Quasi-optical transmission line of the fast ion millimetre wave collective Thomson scattering diagnostics on TEXTOR and ASDEX Upgrade

E. L. Tsakadze, H. Bindslev and S. Michelsen
erekle.tsakadze@risoe.dk

The CTS diagnostic system includes quasi-optical transmission lines and antennae for sending the probing radiation into the plasma and collecting the scattered radiation. The measurement volume in the plasma is the intersection between the probe and the receiver antenna patterns, or beams. The directions and shapes of the beams determine the size and location of the scattering volume. The orientations of the beams, which are variable, in fact also determine which direction in ion velocity space is resolved. Careful design, construction, alignment and quality assurance of the transmission lines and antennae are thus important not only to achieve low loss transmission, but also to provide good spatial localisation of the measurement and accurate definition of the location of the movable measurement volume and resolved velocity direction.

At Risø the desired steerable beam patterns and quasi-optical transmission lines are designed using quasi-optics design tools written in MatLab. These define the quasi-optical mirror shapes, typically ellipsoidal and hyperboloidal surfaces, as well as overmoded corrugated waveguides and scalar horns. For adding engineering details and easy interface with CNC cutting tools, the numerical definitions of reflecting surfaces, waveguides and horns are transferred to the design tool, CATIA. The whole procedure of the mirror production from MatLab to metal can take as little as a few hours. Produced mirror shapes can be characterized by the surface analyser at Risø workshop (see Figure 9).

After construction, the transmission line is aligned with the use of a laser-beam co-linear with the millimetre wave beam centre. For that purpose each mirror contains an optical quality pin located where the centre of the beam should hit the mirror. Properties of the beam are measured at two different locations along the each beam sections with a measuring rig constructed at Risø (see Figure 10).

By the process outlined here, the elements required to intercept the new ECRH transmission line at ASDEX Upgrade for use as a CTS receiver line were designed, constructed and tested at Risø. December 2003 the components were shipped and installed at ASDEX Upgrade at IPP Garching (see Figure 7 and Figure 8 in subsection 2.4.2). The complete alignment of the CTS system will be performed after completion and alignment of the ECRH transmission line (see also subsection 1.1.2).

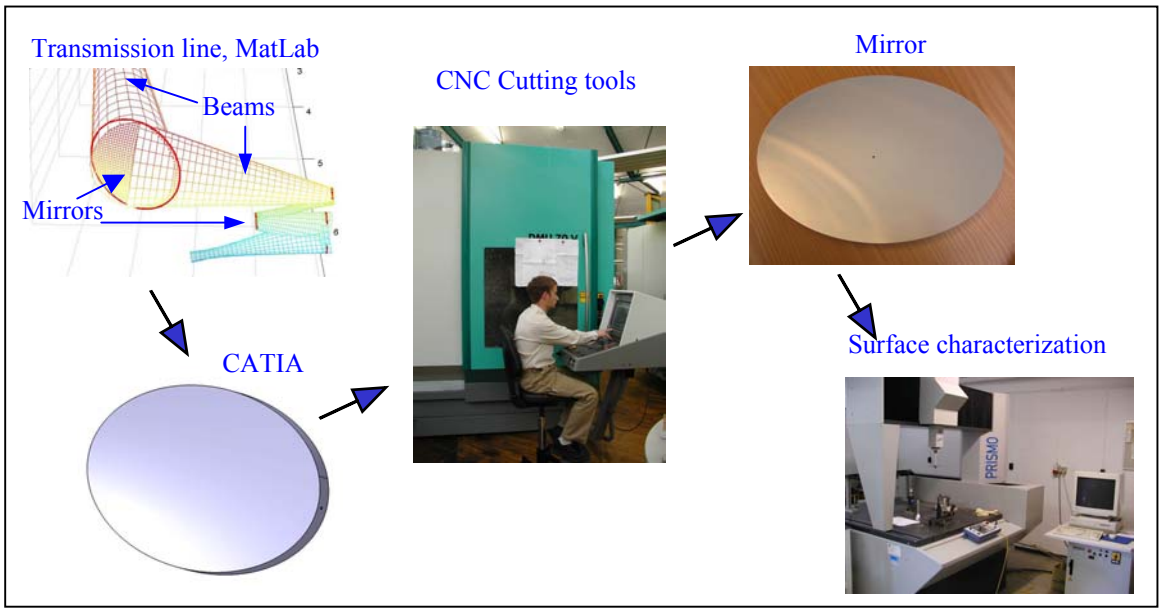

Figure 9. Production of the quasi-optical mirrors from MatLab to metal.

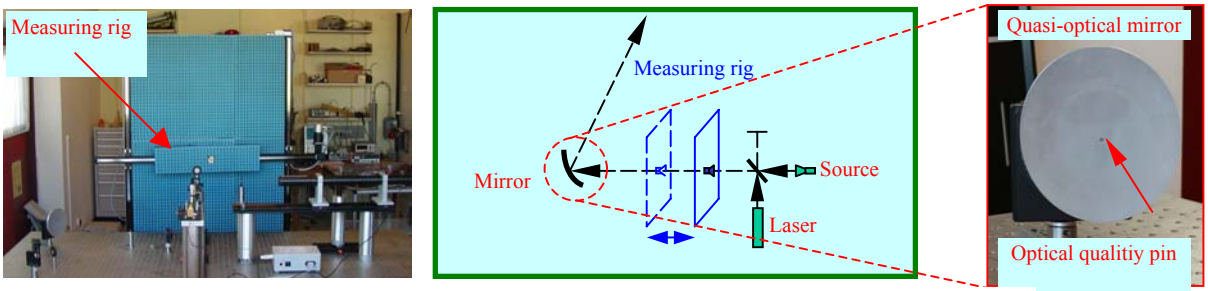

Figure 10. Alignment of the quasi-optical transmission line.

For the upgrade of the TEXTOR CTS system, described in subsection 1.1.1 a full quasi-optical transmission line, including in-vessel steerable antenna, has been designed, and is currently being constructed and tested at Risø.

2.4.4 Electronics for the CTS diagnostics at ASDEX Upgrade and TEXTOR

S. B. Korsholm (also at MIT Plasma Science and Fusion Center, Massachusetts, USA), H. Bindslev, P. K. Michelsen, and P. Woskov (MIT Plasma Science and Fusion Center, Massachusetts, USA)
soeren.korsholm@risoe.dk

While the probe power for a CTS diagnostic is in the order of 100 kW to 1 MW, the power of interest in the scattered spectrum is in the order of 1 nW. The background noise is 10-1000 times the CTS signal. These circumstances set high requirements for the electronics in the CTS receiver.

The electronics of the pilot project TEXTOR CTS system needed an upgrade. A diagram of that receiver is presented in Figure 11. The items marked in blue have been installed as new, while some other components have been upgraded.

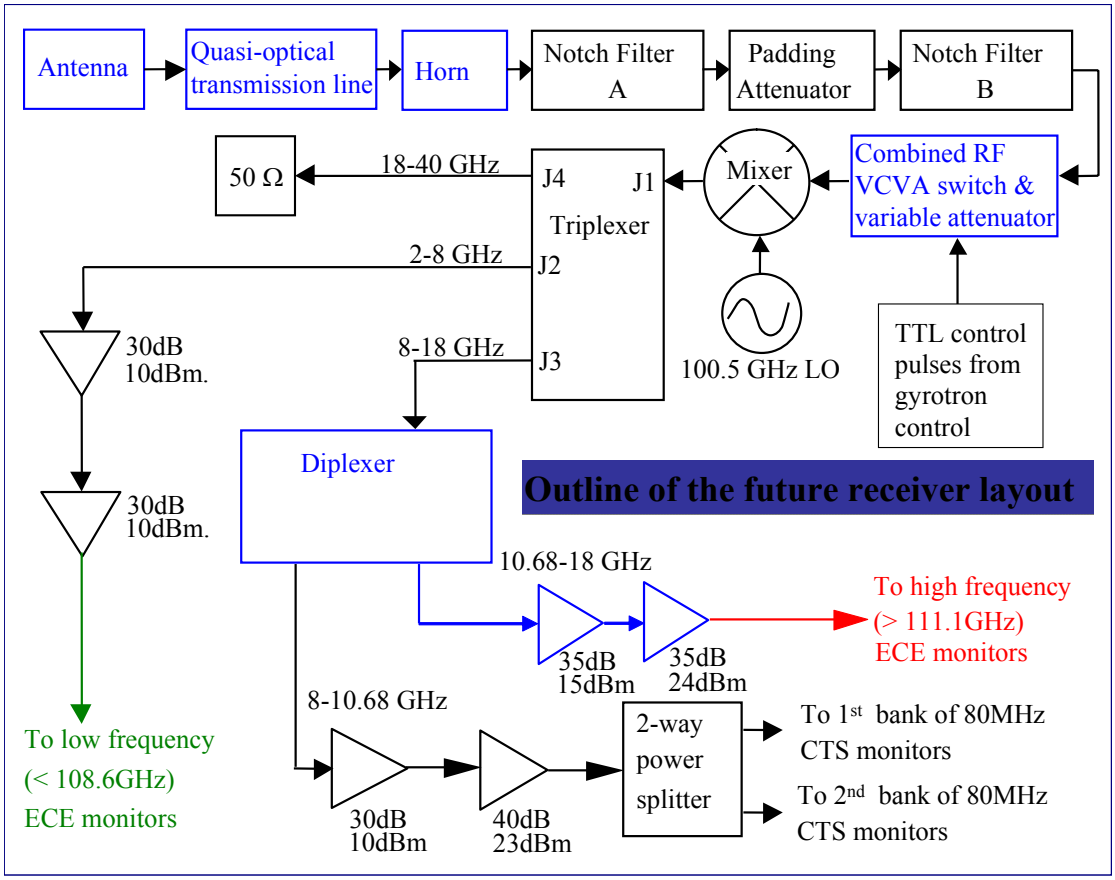

Figure 11. Layout of the electronics in the TEXTOR CTS receiver. Items marked in blue are new for the upgrade of the system.

Some of the main components are the notch filters, following immediately after the horn that interfaces the quasi-optical transmission line and the receiver box. The notch filters attenuate the stray light by damping a 250 MHz band around 110 GHz by 120 dB. After the waveguide components the signal is down-converted by 100.5 GHz, and then split into three bands by a triplexer (actually two diplexers combined), one being the centre part of the spectrum, containing most of the energy, and the other two bands for the lower and upper frequencies. The splitting is done in order to avoid saturation of the amplifiers, which amplifies the signal in each frequency band by 60-70 dB, and to spectrally separate the sensitive wings of the CTS spectrum from the stray light from the probe. Finally, the signal enters filter banks and the data acquisition system described in subsection 2.4.5. The amplifiers are the most delicate parts with specifications like: frequency band 10 to 16 GHz, gain 35 to 40 dB, output power of +15.9 dBm at 1 dB gain compression and a noise figure below 1.8 dB.

The receiver for the ASDEX Upgrade CTS system was designed and built at Risø. The scheme is very similar to that of the TEXTOR system though the physical layout is somewhat different. Figure 12 shows a photograph of the receiver box for the ASDEX Upgrade CTS.

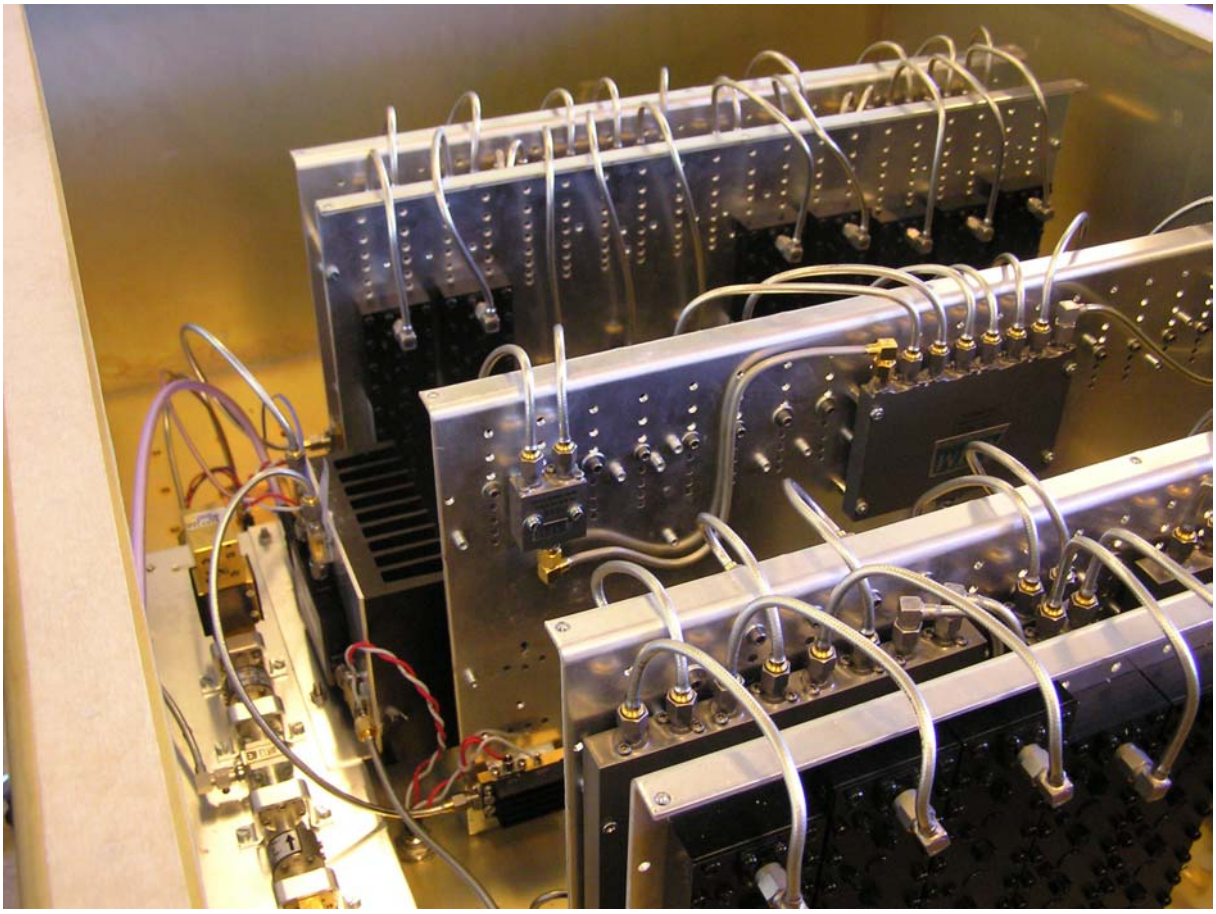

Figure 12. Photo of the ASDEX Upgrade CTS receiver. The filter banks are located to the right and the high frequency (105 GHz) waveguide components to the left.

2.4.5 Data acquisition software and calibration for collective Thomson scattering

S.K. Nielsen, J. Fold von Bülow and P.K. Michelsen
stefan.kragh.nielsen@risoe.dk

The Collective Thomson Scattering systems presently being installed on the fusion research devices ASDEX and TEXTOR (se subsections 2.4.1 and 2.4.2) require a high resolution and synchronized fast scan rate data acquisition system. The hardware and software interaction is therefore crucial.

Two data acquisition systems have been developed using National Instruments NI-4472 PCI cards (8 cards for ASDEX and 7 for TEXTOR), each card with 8 channels with 24-bit resolution and a sampling rate of 102400 Hz. All channels sample synchronously. Each system has an additional NI-6040 card with 16 channels for monitoring system settings such as antenna orientations.

Data Acquisition Software to control the two systems has been developed in "Labview". The software controls the acquiring of data (up to 500MB per plasma discharge) and may run independently of user interaction. The software is capable of performing system calibration and controlling secondary devices such as mirror positions.

The system calibration is carried out by measuring the black body radiation emitted by a warm and a cold source. The difference in signal then yields both the signal gain and the noise in the various channels induced by the system. This noise is expressed as a noise temperature and varies for different channels. The warm source can be a room temperature object or the machine vessel itself. The cold source used is *EchoSorb* submersed in liquid nitrogen. The

alternation between the two sources is done automatically by inserting a mirror just after the horn (se subsections 2.4.1 and 2.4.2).

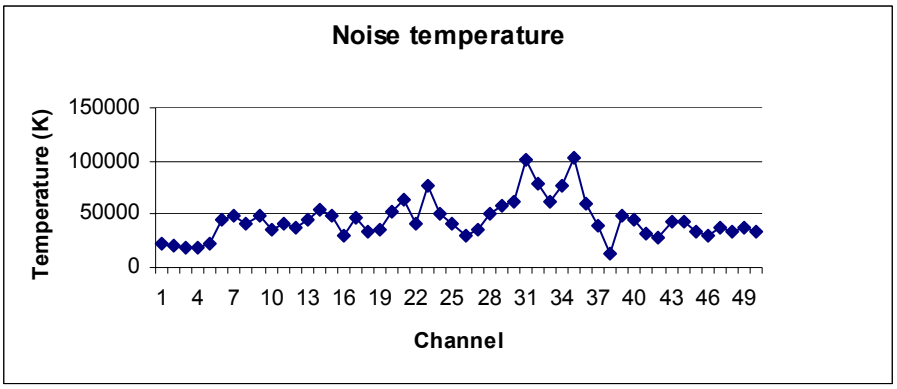

Figure 13. Noise temperature for ASDEX detection system.

An example of measured noise temperature of the ASDEX detection system is given in Figure 13. Here *EchoSorb* in liquid nitrogen was used as the cold source and room temperature *EchoSorb* was used as the warm source.

2.4.6 Diagnosing fast ions in ITER by collective Thomson scattering, feasibility study covering systems from millimetre waves to far infra red

H. Bindslev, F. Meo and S.B. Korsholm
henrik.bindslev@risoe.dk
www.risoe.dk/euratom/cts/ITER

The group conducted an extensive study of the feasibility of measuring the fast ion phase space distribution in ITER by collective Thomson scattering (CTS). The study includes the full range of potential probe frequencies from the gyrotron based mm-wave range, over the far infra-red with sources such as optically pumped molecular lasers and free electron lasers, to the infra-red range of the CO_2 laser. It is assessed whether the systems can meet the ITER measurement requirements and which technological developments may be required. The relative merits of the systems are compared. These include both the achievable resolutions in space, velocity space and time, and accuracies with which these measurements can be obtained. Comparison of systems was preceded by conceptual designs of individual systems to optimise for robustness, resolution and sensitivity, taking technical constraints and potential future enhancements into account.

The study reveals that a CTS system based on a 60 GHz probe frequency, which is below the lower frequency limit of the electron cyclotron emission (ECE) spectrum, has the highest diagnostic potential, and is the only system expected to be able to meet all the ITER fast ion measurement requirements with existing or near term technology.

Collective Thomson scattering cannot distinguish between alpha particles and deuterons travelling at the same velocity, though the signal per alpha particle is four times that of a deuteron. In the direction of the magnetic field and perpendicular to the field deuterons injected by the neutral beam heating system will give rise to fast deuteron populations which will be indistinguishable from the alpha particle population in the velocity range where they overlap. In the direction opposite to the magnetic field (actually opposite to the plasma current), the so-called *counter direction*, the beam deuteron population is negligible. While the dynamics of deuterons and alphas are much alike and both important, it is valuable also to be able to observe the alpha population solely. This is possible in the counter direction. If as expected the population is near isotropic, observation in just one direction defines the full

alpha distribution. With these considerations in mind it is significant that the 60 GHz CTS system permits the counter passing part of the fusion alpha distribution, not obscured by beam ions, to be measured with a spatial resolution of one tenth the minor radius. The conceptual design is presented below in subsection 2.4.7. On the basis of this design costs have been estimated following ITER standard procedures. With modest additions this system may also provide measurements of the fuel ion ratio.

2.4.7 Preliminary design studies of a 60 GHz CTS diagnostic for ITER

F. Meo and H. Bindslev
fernando.meo@risoe.dk

The feasibility study reported in subsection 2.4.6 concludes that a fast ion collective Thomson scattering (CTS) diagnostic with a probe frequency below the electron cyclotron emission spectrum is the only CTS diagnostic capable of meeting the ITER measurement requirements for the fusion alphas, with present or near term technology. The collective Thomson scattering diagnostic for ITER at the 60 GHz range is capable of measuring the fast ion distribution parallel and perpendicular to the magnetic field at different radial locations simultaneously. The design is robust technologically with no moveable components near the plasma. The fast ion CTS diagnostic proposed consists of two separate systems. Each system has its own probe launcher and separate sets of receiving antennae and receivers. The first system, shown in Figure 14, measures the fast ion velocity distribution resolved in the direction perpendicular to the confining magnetic field. For this system the probe and receiver beams are near perpendicular to the magnetic field. The antennae of the probe and receivers are located in the equatorial port on the low field side (LFS)[2].

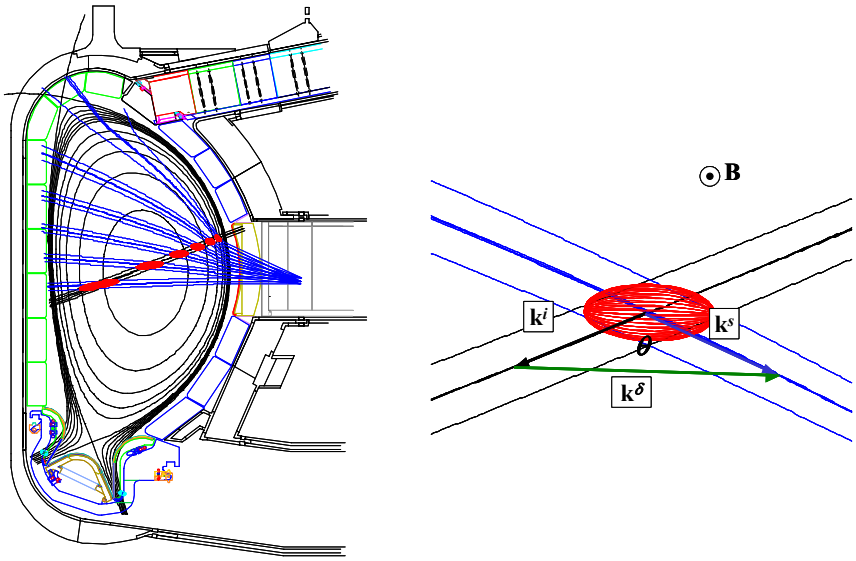

Figure 14. Poloidal view of the LFS-BS set-up: (a) Beam traces of the LFS-BS system w.r.t the ITER vessel components. The probe is in black, receiver beam traces in blue, and the calculated scattering volume in red. (b): A close up view of the probe beam (black), one of the receiver beams (blue), the scattering volume (red). The drawing shows the wave vectors of the received scattered radiation k^s, probe radiation k^i, and the fluctuation wave vector k^δ. ($k^\delta = k^s - k^i$).

[2] The low field side is the side of the plasma or vacuum vessel which has the largest distance to the machine centre and hence the largest major radius.

The receiver consists of a fixed quasi-optical mirror that measures backscattered radiation and couples it to a distributed set of receiver horns. This system is referred to by the acronym LFS-BS system referring to the location of the receiver and the fact that it measures backscattered radiation. Figure 15 shows a schematic of the front-end of the probe launcher and the receiver of the LFS-BS system. It shows the receiver consisting of a quasi-optical mirror coupled to an array of horns mounted in a stainless steel frame that houses a series of fundamental waveguides connected to the horns. The waveguides are directed to tapers coupled to over-moded waveguides. Each horn is located at a different distance from the mirror and collects scattered radiation from a different radial position in the plasma, as shown by the dotted and solid blue lines in Figure 15.

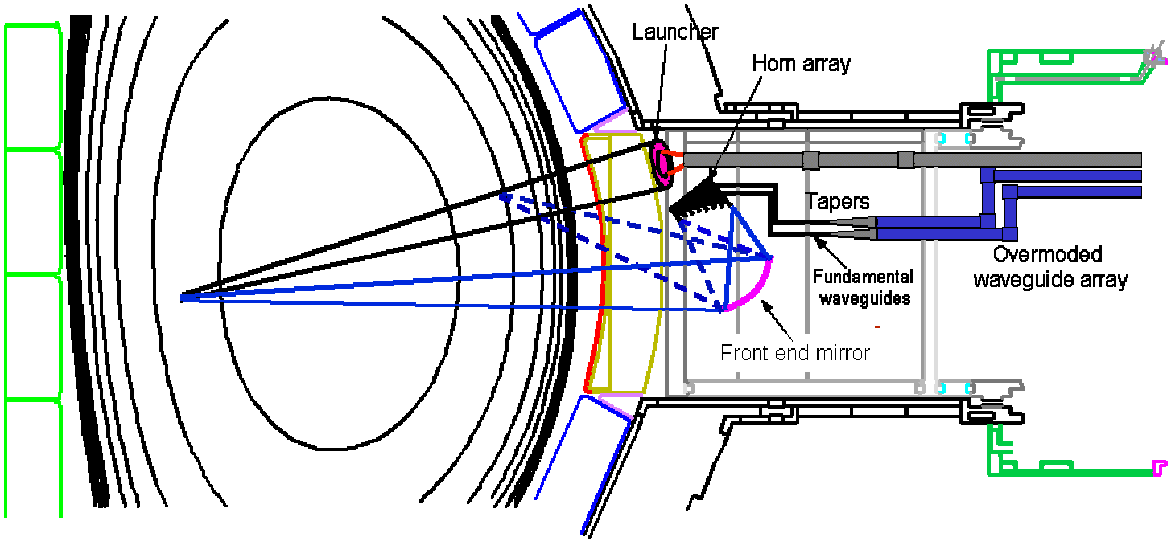

Figure 15. Schematic of the side view of the LFS-BS components. The probe launchers are located in the same poloidal plane as the detectors.

The second part of the CTS diagnostic, shown in Figure 16, measures fast ion velocity distribution resolved in the direction parallel to the confining magnetic field. It consists of a probe launcher located in the low field side mid-plane port and a receiver array located on high field side. This system will be referred to as HFS-FS referring to the location of the receivers and that they measure forward scattered radiation.

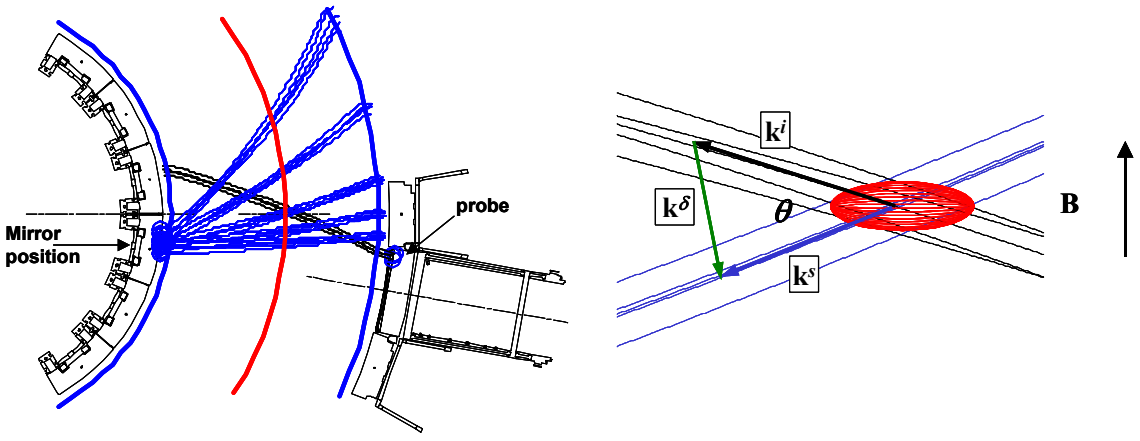

Figure 16. (a) Top view of beam traces for the HFS-FS with a LFS probe launcher (black) and HFS detectors (blue). The red curve indicates the plasma centre. (b) Close up view of the probe beam and one of the receiver beams with the scattering volume in red. Shown are the wave vectors of the received scattered radiation k^s, the incident probe radiation k^i, and the fluctuation vector $k^\delta = k^s - k^i$. which is near parallel to B.

The hardware of the HFS receivers consists of a quasi-optical mirror mounted on the inner vessel wall below the blanket module key as shown in the side view sketch in Figure 17a. Toroidally the mirror is located between the cooling manifolds (Figure 17b). The mirror collects scattered radiation from a narrow horizontal slot between blanket modules which form the first wall against the plasma. The mirror relays the radiation to a series of horns. The horns are distributed toroidally, each representing a different toroidal angular view in the plasma. The horns are encased inside a cast, housing fundamental waveguides that are routed upwards along the inner vessel wall. These are in turn coupled to over-moded waveguides that run up along the vacuum vessel wall behind the blanket modules toward the upper port.

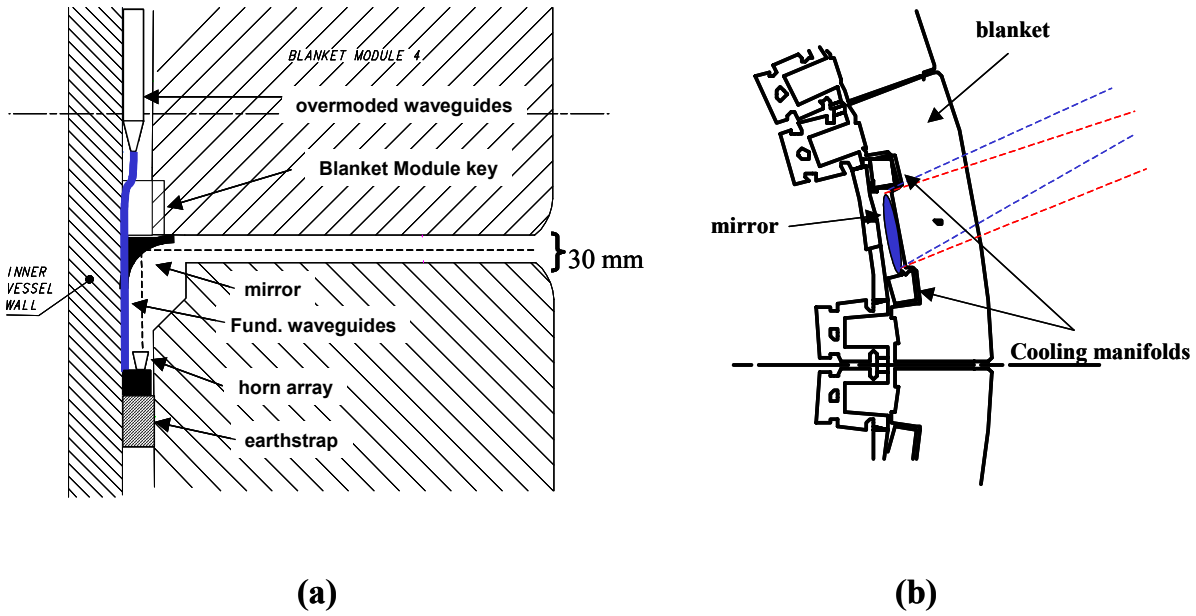

Figure 17. (a) Cross section of blanket modules 3 and 4 with mirror, horn array, and waveguide assembly. The vertical distance between the blanket modules gap diameter is 30 mm as shown. (b) Top view of mirror located behind the blanket module between the cooling manifolds.

In close collaboration with the ITER International Team, the preliminary phase of the hardware design for the CTS on ITER has been completed. The 3-D CATIA drawings in Figure 18(a) show the view of ITER's equatorial port #12 with the blanket and the apertures for the CTS. In Figure 18(b), the blanket module is not shown and the plug front plate was made semi-transparent in this illustration for a better view of the front-end optics and the port plug waveguides. The launcher for both the LFS-BS and HFS-FS system consists of two fixed quasi-optical ellipsoidal mirrors fed by a corrugated high power waveguide. The purple and orange dash-dotted line shows the beam centre of the LFS-BS probe and the HFS-FS probe respectively. Also shown are the first mirror and the horn array of the LFS-BS receiver. The enclosure in blue contains the fundamental waveguides that are directed to tapers and are couple to the over-moded waveguides. Not shown in this report is the preliminary hardware design for the HFS-FS receiver located on the inner vessel wall. There is no integration issues with other diagnostics yet identified in port #12. A relatively low cost upgrade to the LFS-BS system of CTS has the potential to provide temporally and spatially resolved measurements of the fuel ion ratio.

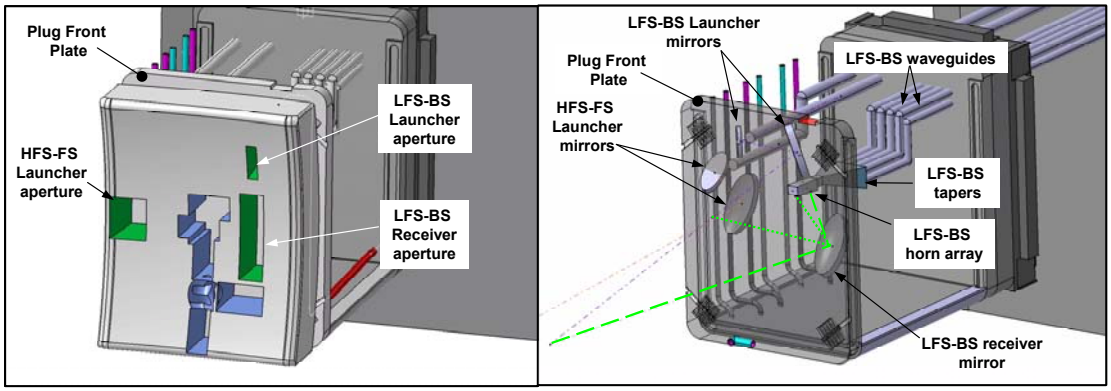

Figure 18. (a) View from the plasma side of the mid plane port plug #12. The apertures for the CTS diagnostic are shown in green. The apertures in blue are for the other diagnostics that share the same port. (b) View of the CTS in port plug from the plasma side without the blanket module.

2.5 Publications and conference contributions

2.5.1 International publications

Basse, N.P.; Zoletnik, S.; Antar, G.Y.; Baldzuhn, J.; Werner, A., Characterization of turbulence in L- and ELM-free H-mode Wendelstein 7-AS plasmas. *Plasma Phys. Control. Fusion* (2003) **45** , 439-453

Basse, N.P.; Zoletnik, S.; Baumel, S.; Endler, M.; Hirsch, M.; McCormick, K.; Werner, A., Turbulence at the transition to the high density H-mode in Wendelstein 7-AS plasmas. *Nucl. Fusion* (2003) **43** , 40-48

Basu, R.; Naulin, V.; Juul Rasmussen, J., Particle diffusion in anisotropic turbulence. *Commun. Nonlinear Sci. Num. Simul.* (2003) **8** , 477-492

Basu, R.; Jessen, T.; Naulin, V.; Juul Rasmussen, J., Turbulent flux and the diffusion of passive tracers in electrostatic turbulence. *Phys. Plasmas* (2003) **10** , 2696-2703

Bian, N.H.; Garcia, O.E., Confinement and dynamical regulation in two-dimensional convective turbulence. *Phys. Plasmas* (2003) **10** , 4696-4707

Garcia, O.E.; Bian, N.H., Bursting and large-scale intermittency in turbulent convection with differential rotation. *Phys. Rev. E* (2003) **68** , 047301.1-047301.4

Garcia, O.E.; Bian, N.H.; Paulsen, J.V.; Benkadda, S.; Rypdal, K., Confinement and bursty transport in a flux-driven convection model with sheared flows. *Plasma Phys. Control. Fusion* (2003) **45** , 919-932

Guio, P.; Børve, S.; Daldorff, L.K.S.; Lynov, J.P.; Michelsen, P.; Pecseli, H.L.; Juul Rasmussen, J.; Saeki, K.; Truelsen, J., Phase space vortices in collisionless plasmas. *Nonlinear Process. Geophys.* (2003) **10** , 75-86

Krolikowski, W.; Bang, O.; Wyller, J.; Juul Rasmussen, J., Optical beams in nonlocal nonlinear media. *Acta Phys. Pol. A* (2003) **103** , 133-147

Naulin, V.; Nielsen, A.H., Accuracy of spectral and finite difference schemes in 2D advection problems. *SIAM J. Sci. Comput.* (2003) **25** , 104-126

Naulin, V., Electromagnetic transport components and sheared flows in drift-Alfven turbulence. *Phys. Plasmas* (2003) **10** , 4016-4028

Naulin, V.; Juul Rasmussen, J.; Nycander, J., Transport barriers and edge localized modes-like bursts in a plasma model with turbulent equipartition profiles (Erratum in Phys. Plasmas v. 9, 3804 (2003)). *Phys. Plasmas* (2003) **10** , 1075-1082

Verhoeven, A.G.A.; Bongers, W.A.; Elzendoorn, B.S.Q.; Graswinckel, M.; Hellingman, P.; Kooijman, W.; Kruijt, O.G.; Maagdenberg, J.; Ronden, D.; Stakenborg, J.; Sterk, A.B.; Tichler, J.; alberti, S.; Goodman, T.; Henderson, M.; Hoekzema, J.A.; Oosterbeek, J.W.; Fernandez, A.; Likin, K.; Bruschi, A.; Cirant, S.; Novak, S.; Piosczyk, B.; Thumm, M.; Bindslev, H.; Kaye, A.; Fleming, C.; Zohm, H., The design of an ECRH system for JET-EP. Nucl. Fusion (2003) **43** , 1477-1486

2.5.2 Danish publications

Bindslev, H.; Singh, B.N (eds.), Association Euratom - Risø National Laboratory annual progress report 2002. Risø-R-1414(EN) (2003) 53 p.

2.5.3 Conference lectures

Bindslev, H., Operations space diagram for ECRH and ECCD in JET and ITER. In: Proceedings. 12. Joint workshop on electron cyclotron emission and electron cyclotron resonance heating, Aix-en-Provence (FR), 13-16 May 2002. (World Scientific, Singapore, 2003) p. 119-124

Garcia, O.E.; Bian, N.H.; Naulin, V.; Nielsen, A.H.; Juul Rasmussen, J., Bursting and intermittency in two-dimensional convective turbulence (poster). In: Contributed papers (on CD-ROM). 30. European Physical Society conference on controlled fusion and plasma physics, St. Petersburg (RU), 7-11 Jul 2003. (European Physical Society, Paris, 2003) (Europhysics Conference Abstracts, vol. 27A) P-1.173 (4 p.)

Korsholm, S.B.; Bindslev, H.; Egedal, J.; Hoekzema, J.A.; Leuterer, F.; Meo, F.; Michelsen, P.K.; Tsakadze, E.L.; Woskov, P., Fast ion millimeter wave CTS diagnostics on TEXTOR and ASDEX upgrade (poster). In: Contributed papers (on CD-ROM). 30. European Physical Society conference on controlled fusion and plasma physics, St. Petersburg (RU), 7-11 Jul 2003. (European Physical Society, Paris, 2003) (Europhysics Conference Abstracts, vol. 27A) P-1.53 (4 p.)

Michelsen, P.K.; Bindslev. H.; Hansen, R.S.; Hanson, S.G., Position control of ECRH launcher mirrors by laser speckle sensor. In: Proceedings. 12. Joint workshop on electron cyclotron emission and electron cyclotron resonance heating, Aix-en-Provence (FR), 13-16 May 2002. (World Scientific, Singapore, 2003) p. 553-558

Naulin, V., Electromagnetic transport components and sheared flows in plasma edge turbulence (invited topical talk). In: Proceedings (CD-ROM). 11. International congress on plasma physics (ICPP 2002), Sydney (AU), 15-19 Jul 2002. Falconer, I.S.; Dewar, R.L.; Khachan, J. (eds.), (American Institute of Physics, New York, 2003) (AIP Conference Proceedings, 669) p. 626-629

Naulin, V.; Nycander, J.; Juul Rasmussen, J., Dynamics of transport barriers and ELM-like behaviour in electrostatic turbulence (poster). In: Proceedings (CD-ROM). 11. International congress on plasma physics (ICPP 2002), Sydney (AU), 15-19 Jul 2002. Falconer, I.S.; Dewar, R.L.; Khachan, J. (eds.), (American Institute of Physics, New York, 2003) (AIP Conference Proceedings, 669) p. 659-661

Naulin, V.; Juul Rasmussen, J., Aspects of turbulent transport (invited paper). In: Proceedings. Vol. 4. International conference on phenomena in ionized gases (26. ICPIG), Greifswald (DE), 19-20 Jul 2003. Meichsner, J.; Loffhagen, D.; Wagner, H.-E. (eds.), (Local Organizing Committee, Greifswald, 2003) p. 237-238

Naulin, V.; Garcia, O.E.; Nielsen, A.H.; Juul Rasmussen, J., Statistics of SOL and drift-wave turbulence transport events. In: Contributed papers (on CD-ROM). 30. European Physical Society conference on controlled fusion and plasma physics, St. Petersburg (RU), 7-11 Jul 2003. (European Physical Society, Paris, 2003) (Europhysics Conference Abstracts, vol. 27A) O-2.4A (4 p.)

Verhoeven, A.G.A.; Bongers, W.A.; Elzendoorn, B.S.Q.; Graswinckel, M.; Hellingman, P.; Kamp, J.J.; Kooijman, W.; Kruijt, O.G.; Maagdenberg, J.; Ronden, D.; Stakenborg, J.; Sterk, A.B.; Tichler, J.; Alberti, S.; Goodman, T.; Henderson, M.; Hoekzema, J.A.; Oosterbeek, J.W.; Fernandez, A.; Likin, K.; Bruschi, A.; Cirant, S.; Novak, S.; Piosczyk, B.; Thumm, M.; Bindslev, H.; Kaye, A.; Fleming, C.; Zohm, H., The 113 GHz ECRH system for JET. In: Proceedings. 12. Joint workshop on electron cyclotron emission and electron cyclotron resonance heating, Aix-en-Provence (FR), 13-16 May 2002. (World Scientific, Singapore, 2003) p. 511-516

Westerhof, E.; Hogeweij, G.M.D.; Hoekzema, J.A.; Schüller, F.C.; Barth, C.J.; Bindslev, H.; Donné, A.J.H.; Dumortier, P.; Gorkom, J.V. van; Jaspers, R.J.E.; Kalupin, D.; Koslowski, H.R.; Krämer-Flecken, A.; Cardozo, N.J.L.; Meiden, H.J. van der; Messiaen, A.; Oyevaar, T.; Polman, R.W.; Porte, L.; Udintsev, V.S.; Unterberg, B.; Vervier, M.; Eester, D. van; Wassenhove, G. van, Electron cyclotron resonance heating on TEXTOR: Results from the preliminary 110 GHz system. In: Proceedings. 12. Joint workshop on electron cyclotron emission and electron cyclotron resonance heating, Aix-en-Provence (FR), 13-16 May 2002. (World Scientific, Singapore, 2003) p. 395-402

2.5.4 Unpublished Danish lectures

Jensen, V.O., Fusionsenergi - fremtidens uudtømmelige energikilde. Møde i Ungdommens Naturvidenskabelige forening, UNF, Aalborg (DK), 11 Feb 2003.

Jensen, V.O., Fusionsenergi - fremtidens uudtømmelige energikilde. Møde i Ungdommens Naturvidenskabelige forening, UNF, Århus (DK), 11 Sep 2003.

2.5.5 Unpublished international lectures

Bindslev, H., ITER: An opportunity for Europe. Dinner debate on fusion, European Parliament, Strasbourg (FR), 19 Nov 2003.

Bindslev, H., Fast ion dynamics measured by collective Thomson scattering (invited lecture). International conference: Plasma 2003, Warsaw (PL), 9-12 Sep 2003.

Bindslev, H., ECW-CMA operations space diagram for ITER. IAEA technical meeting on ECRH physics and technology for ITER, Kloster Seeon (DE), 14-16 Jul 2003.

Bindslev, H.; Korsholm, S.; Meo, F.; Michelsen, P.; Søgård, S.; Tsakadze, E.; Woskov, P.; Hoekzema, F.; Leuterer, F.; Egedal, J.; Porte, L.; Eester, D. van, Fast ion dynamics measured by collective Thomson scattering. Colloquium IPP Garching, Garching (DE), 16 May 2003.

Bindslev, H.; Tsakadze, E.; Meo, F.; Korsholm, S.; Michelsen, P.; Woskov, P.; Hoekzema, F.; Leuterer, F.; Egedal, J.; Porte, L.; Eester, D. van, Diagnosing fast ions in ITER with collective Thomson scattering. 4. Meeting of the ITPA Topical Group on Diagnostics, Padova (IT), 17-21 Feb 2003.

Garcia, O.E.; Bian, N.H.; Naulin, V.; Nielsen, A.H.; Juul Rasmussen, J., Bursting and intermittency in two-dimensional convective turbulence. Meeting on new themes in plasma and fluid turbulence, London (GB), 13-14 May 2003.

Garcia, O.E.; Naulin, V.; Nielsen, A.H.; Juul Rasmussen, J., Transport statistics and intermittency in plasma turbulence. In: Book of abstracts. 10. European fusion theory conference (EFTC), Helsinki (FI), 8-10 Sep 2003. (Helsinki University of Technology, Helsinki, 2003) p. O-6 (P2-9)

Garcia, O.E.; Naulin, V.; Nielsen, A.H.; Juul Rasmussen, J., Theoretical investigation on intermittent transport in the scrape-off-layer (poster). In: Book of abstracts. 10. European fusion theory conference (EFTC), Helsinki (FI), 8-10 Sep 2003. (Helsinki University of Technology, Helsinki, 2003) p. P2-23

Juul Rasmussen, J., Self-focusing and wave collapse dynamics. Seminar at College of Charleston, Charleston, SC (US), 2003.

Juul Rasmussen, J.; Naulin, V.; Basu, R.; Jessen, T., Particle diffusion and transport in electrostatic turbulence. Meeting on new themes in plasma and fluid turbulence, London (GB), 13-14 May 2003.

Korsholm, S.B., Fast ion millimeter wave CTS diagnostics on TEXTOR and ASDEX upgrade. Seminar at ELVA-1 Millimeter Wave Division (DOK Ltd.), St. Petersburg (RU), 10 Jul 2003.

Korsholm, S.B.; Bindslev, H.; Egedal, J.; Hoekzema, J.; Leuterer, F.; Meo, F.; Michelsen, S.; Michelsen, P.K.; Tsakadze, E.L.; Woskov, P., Implementation of fast ion millimeter wave CTS diagnostics on TEXTOR and ASDEX upgrade. 45. Annual meeting of the Division of Plasma Physics, American Physical Society, Albuquerque, NM (US), 27-31 Oct 2003.

Korsholm, S.B.; Bindslev, H.; Egedal, J.; Hoekzema, J.A.; Leuterer, F.; Michelsen, P.K.; Tsakadze, E.; Woskov, P., Fast ion millimeter wave CTS diagnostics on TEXTOR and ASDEX (poster). In: Program. 44. Annual meeting of the Division of Plasma Physics, American Physical Society, Orlando, FL (US), 11-15 Nov 2002. (American Institute of Physics, Melville, NY, 2002) (Bulletin of the American Physical Society, v. 47, no. 9) p. 84

Milovanov, A.V.; Juul Rasmussen, J., Topology of percolation at criticality and the Alexander-Orbach conjecture. Niels Bohr Summer Institute on complexity and criticality symposium and workshop, Copenhagen (DK), 21-29 Aug 2003.

Naulin, V., Turbulence, flows, transport .... Risø's 2 cent worth. IPP Theorie meeting, Mac-Planck Gesellschaft, Zinnowitz (DE), 17-20 Nov 2003.

Naulin, V.; Garcia, O.E.; Nielsen, A.H.; Basu, R.; Juul Rasmussen, J., Transport statistics in drift-wave turbulence (poster). Niels Bohr Summer Institute on complexity and criticality symposium and workshop, Copenhagen (DK), 21-29 Aug 2003.

Naulin, V.; Garcia, O.E.; Nielsen, A.H.; Basu, R.; Juul Rasmussen, J., Transport statistics in drift-wave turbulence. Meeting on new themes in plasma and fluid turbulence, London (GB), 13-14 May 2003.

Naulin, V.; Basu, R.; Garcia, O.E.; Nielsen, A.H.; Juul Rasmussen, J., Statistics of transport in drift and drift-Alfvén turbulence (invited talk). 8. Easter plasma meeting, Torino (IT), Apr 2003.

Nielsen, A.H.; Garcia, O.E.; Naulin, V.; Juul Rasmussen, J., Fluctuation statistics from numerical simulations of scrape-off-layer. Meeting on new themes in plasma and fluid turbulence, London (GB), 13-14 May 2003.

Ramponi, G.; Bindslev, H.; Farina, D.; Giruzzi, G.; Lloyd, B.; Novak, S.; Poli, E.; Shevchenko, V.; Volpe, F.; Zohm, H., Optimisation of the ITER top launcher. IAEA technical meeting on ECRH physics and technology for ITER, Kloster Seeon (DE), 14-16 Jul 2003

Schröder, C.; Grulke, O.; Klinger, T.; Naulin, V., Investigations on drift wves in a helicon discharge (poster). Spring meeting of the German Physical Society DPG, Section Plasma Physics, Aachen (DE), 10-13 Mar 2003.

3. Fusion technology

3.1 Introduction

The work reported in this section has been carried out in the Materials Research Department. The overall objective of the research activities in this area is to determine the impact of neutron irradiation on physical and mechanical properties of metals and alloys, so that appropriate materials can be chosen for their application in irradiation environment (e.g. in fusion reactor). Various experimental techniques are employed to study different aspects of the microstructural evolution during irradiation and the resulting consequences of the post-irradiation physical and mechanical properties of metals and alloys. Calculations and computer simulations are performed to understand the evolution of surviving defects and their clusters in collision cascades. The kinetics of defect accumulation during irradiation and the influence of irradiation-induced defects and their clusters on the deformation behaviour of irradiated metals and alloys are studies theoretically. In the following, the main results of these activities are highlighted.

3.2 Next step technology

3.2.1 In-reactor tensile testing of pure copper and CuCrZr alloy in the BR-2 reactor at Mol[3]

B.N. Singh, S. Tähtinem, P. Moilanen* (VTT Industrial Systems (Association EURATOM-TEKES), Espoo, Finland), P. Jacquet**, J. Dekeyser** (Reactor Experiment Department, SCK.CEN, Mol, Belgium) and D.J. Edwards*** (Pacific Northwest National Laboratory, Richland, USA)*

Experimental activities on determining the deformation behaviour of copper and copper alloys under the dynamic conditions of simultaneous mechanical loading and neutron irradiation were continued. Results of the first such an in-reactor tensile test were reported last year[4,5,2,3]. Since then, more in-reactor tensile tests have been carried out and the main results are summarised below.

Materials used in the present investigations were thin (0.3 mm) sheets of (a) oxygen-free-high conductivity (OFHC) copper and (b) prime aged (460°C for 3h) CuCrZr alloy supplied by Outokumpu OY (Finland). Prior to irradiation, the polycrystalline OFHC-Cu specimens were annealed at 550°C for 2 h in a vacuum of 10^{-9} bar.

The in-reactor tensile tests were carried out in specially designed pneumatically controlled test modules. Prior to irradiation, test modules were calibrated out-of-pile. Two test modules, each containing one tensile specimen, were loaded in one irradiation rig. The applied stress and the resulting strain on each specimen were measured separately. Both stress and strain were measured continuously throughout the whole experiment both in the case of out-of-pile and in-reactor tests. The temperature of the experiments was measured and recorded continuously. Two sets of tensile tests are carried out.

---

[3] Task TW2-TVM-SITU

[4] Risø Report No. Risø-R-1414(EN), May 2003, p. 37

[5] B.N. Singh et al., J. Nucl. Mater. 320 (2003) 299

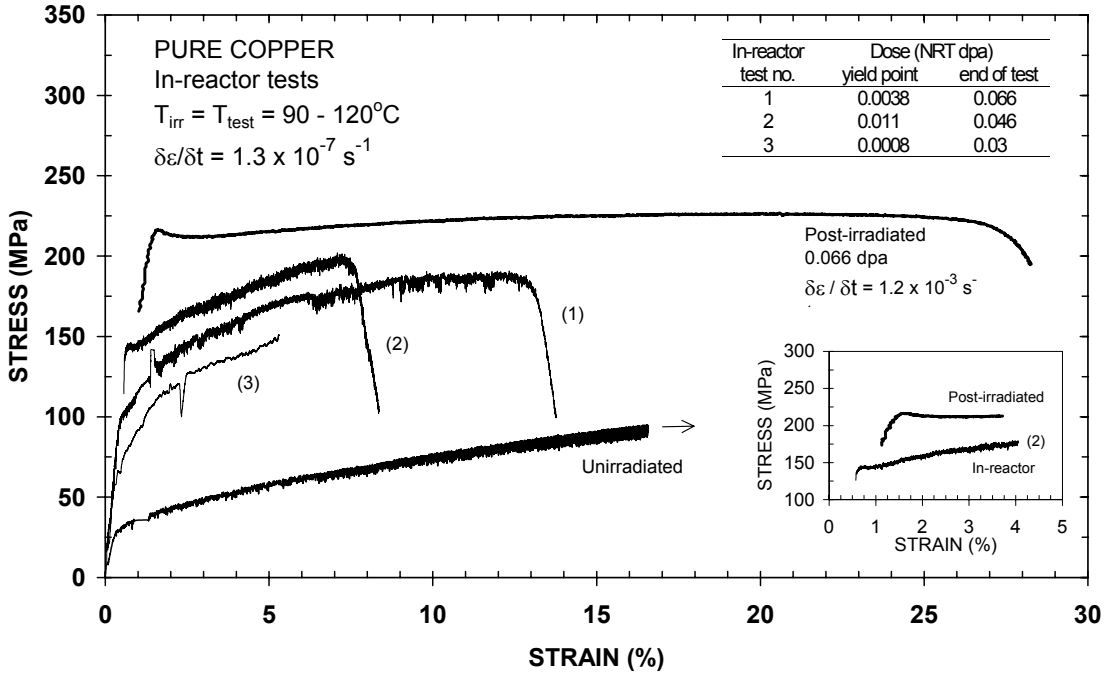

Figure 1. The dynamic response of tensile specimens of OFHC-copper during in-reactor tensile tests showing build-up of stress and strain (curves 1, 2 and 3). For comparison, tensile tests of the reference unirradiated and post-irradiated specimens are also shown. The relevant test parameters are indicated in the figure. Note that the displacement dose increases linearly with increasing strain. Therefore the curves illustrate the combined effect of strain hardening and irradiation hardening.

In the first set of experiments two specimens of OFHC copper (number 1 and 2) were tensile tested at ~90°C with a fast neutron flux of ~$3x10^{17}$n/m^2s (E>1MeV) corresponding to a displacement damage rate of ~$6x10^{-8}$ dpa/s. The specimens were tested at a constant strain rate of 1.3 x 10^{-7} s^{-1} (~1.1% per day). This low strain rate was chosen to ensure that the specimen should survive the in-reactor deformation for long enough to accumulate a displacement dose level of about 0.1 dpa. This was necessary in order to assess the dynamic effects of irradiation and the applied stress on the deformation behaviour of the specimens. The tensile tests were discontinued soon after the specimens showed a clear sign of fracture initiation. The irradiation rig was then taken out of the reactor.

In the second set of experiments, one test module was loaded with another copper tensile specimen (number 3) and the other test module was loaded with a CuCrZr tensile specimen. The test temperature during these tests was about 120°C. The test procedure was the same as that in the case of the first set of experiments.

Figure 1 shows the dynamic engineering stress-strain curves for three copper specimens (marked 1, 2 and 3) measured directly in the reactor during irradiation. These curves illustrate the mechanical response of the material to the simultaneous application of the applied stress and the displacement damage produced by neutrons. It should be noted that the measured increase in the stress level with increasing strain includes also the effect of irradiation dose, since during the experiment, both the irradiation dose and the applied strain increase linearly with irradiation time. In other words, the measured hardening is a combined effect of strain hardening and irradiation hardening. Figure 1 also includes the result of a out-of-pile and post-irradiation tensile test (the top curve) carried oout at 90°C on a copper specimen which was irradiated together with the specimen (1) but without stress and also to a dose level of 0.066 dpa. The bottom curve in Figure 1 shows the result of out-of-pile reference test (i.e. without irradiation) carried out at 90°C at a strain rate of 1.3 x 10^{-7} s^{-1}.

It should be pointed out that different deformation behaviour illustrated by curves (1), (2) and (3) in Figure 1 is due to the fact that these specimens received different levels of displacement doses before the deformation was started (i.e. in the absence of applied stress). The specimen (2) was given the highest (10^{-2} dpa) and (3) the lowest ($<10^{-4}$ dpa) amount of pre-deformation displacement dose. The curves (1), (2) and (3) clearly demonstrate that the pre-deformation damage level has a significant effect on the deformation behaviour (hardening as well as ductility) of materials during irradiation.

The most significant feature of the present results is that during the dynamic in-reactor test, the material deforms uniformly and in a homogeneous fashion and does not show any sign of yield drop and plastic instability, as commonly demonstrated by the post-irradiation experiments.

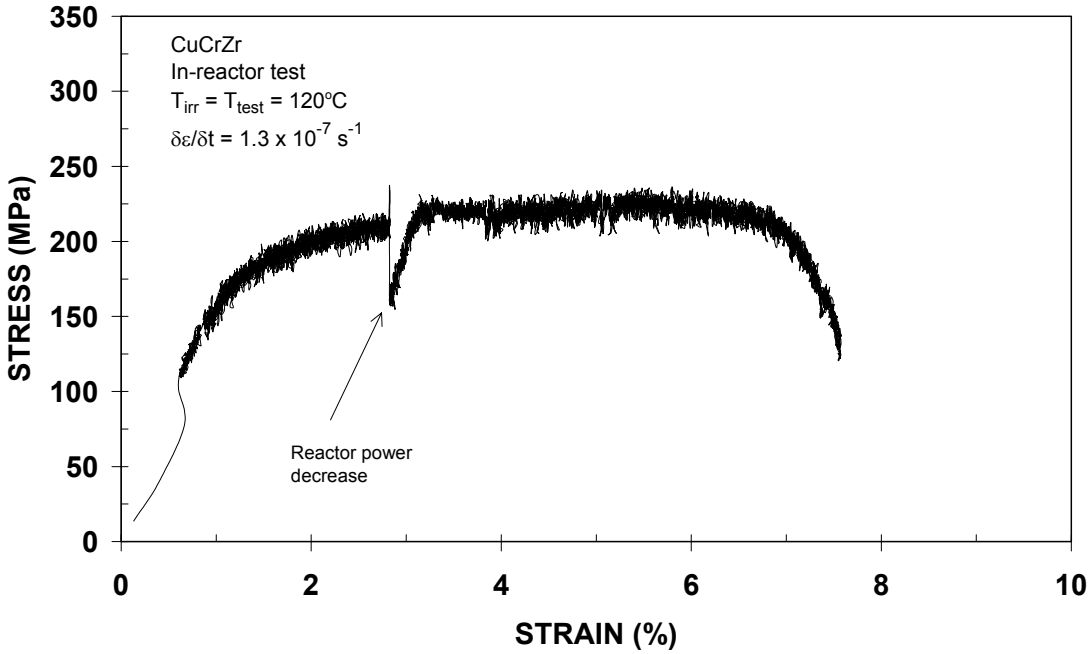

Figure 2. The dynamic response of a tensile specimen of CuCrZr alloy during in-reactor tensile test showing build-up of stress and strain. Like in Figure 1, the curve illustrates the combined effect of strain hardening and irradiation hardening. Note the absence of yield drop and plastic instability.

Figure 2 shows the engineering stress-strain curve obtained during an in-reactor tensile test of a CuCrZr alloy specimen at about 120°C at a nominal strain rate of 1.0×10^{-7} s^{-1} and at a damage rate of ~6×10^{-8} dpa/s. The test procedure was the same as that in the case of copper specimens. The tensile test lasted for 195.5 hours and the accumulated displacement dose during this period was about 0.042 dpa. As can be seen in Figure 2, the deformation occurs smoothly and homogeneously, yielding a total elongation of about 7.5%. Clearly, there is no indication of the occurrence of a yield drop. This is in sharp contrast to the deformation behaviour of CuCrZr alloy commonly observed in the post-irradiation tests.

The microstructure of both OFHC-copper and CuCrZr alloy have been investigated using transmission electron microscopy (TEM) in the unirradiated, as-irradiated as well as in-reactor deformed specimens. The microstructural evolution observed in the in-reactor tensile test is vastly different from that in the case of the out-of-pile tensile test in the absence of irradiation. Figure 3 shows a typical example of dislocation microstructure observed in the out-of-pile test at 90°C at a strain rate of 1.3×10^{-7} s^{-1} to a strain level of 20%. The microstructure of the in-reactor deformed specimen (number 1 in Figure 1) at 90°C to a total strain level of 13.7% is shown in Figure 4. Figure 4(a) illustrates the homogeneous nature of dislocation activities

between the channels whereas Figure 4(b) shows the localisation of plastic deformation in the form of cleared channels. The comparison of Figure 3 and Figure 4 demonstrates the fundamental differences in dislocation generation and motion behaviour between the out-of-pile deformation and the in-reactor deformation experiments.

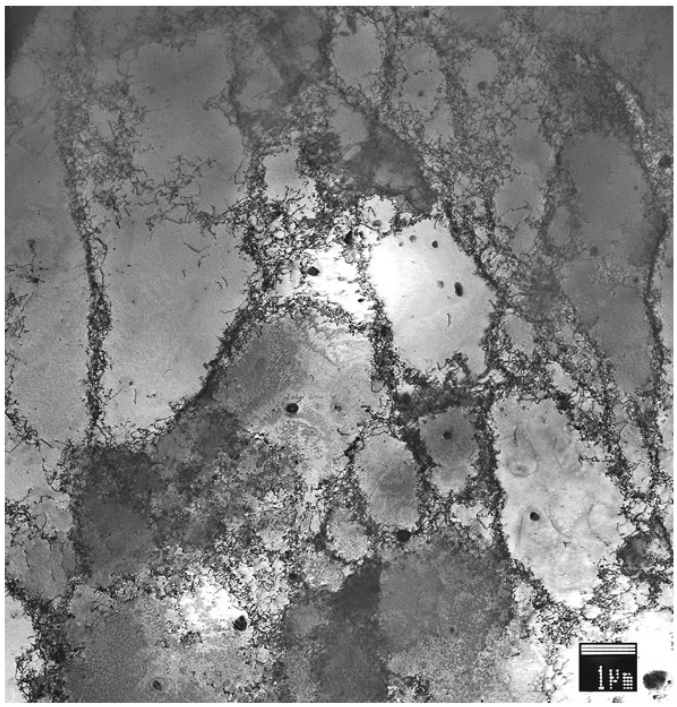

Figure 3. Dislocation microstructure of a OFHC copper specimen tensile tested in the unirradiated condition at a strain rate of 1.3 x 10^{-7} s^{-1} at 90°C to a strain level of 20%. Note the segregation of dislocations in the form of cell walls.

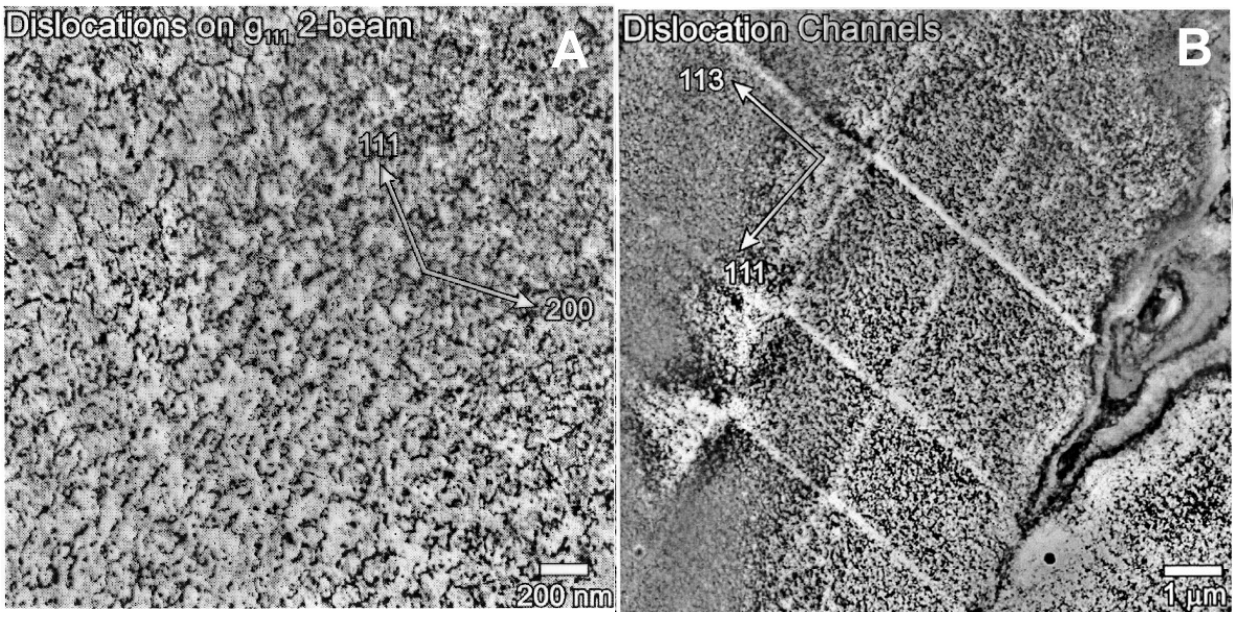

Figure 4. Microstructure of a OFHC-copper specimen in-reactor tensile tested at 90°C to a total strain level of 13.7% (curve 1 in Figure 1) showing (a) dislocation segments and loops between the channels and (b) formation of cleared channels. Note the lack of long distance dislocation transport, dislocation-dislocation interactions and the formation of dislocation walls.

The analysis of these limited number of in-reactor deformation experiments suggests that the mechanical performance of materials exposed simultaneously to stress and irradiation in a reactor environment is likely to be better than expected on the basis of the results obtained from post-irradiated tests. However, more in-reactor experiments are necessary to validate this trend.

3.2.2 Creep-fatigue cyclic deformation and lifetime of CuCrZr alloy[6]

B.N. Singh, B.S. Johansen and L. Korcakova

At present it seems almost certain that the precipitation hardened CuCrZr alloy will be used both in the first wall and divertor components of ITER. In the reactor vessel, this alloy will be exposed to a relatively high flux of 14 MeV neutrons and will experience thermo-mechanical cyclic loading as a result of the cyclic nature of the plasma burn operations of the system. Because of the "plasma-on" and "plasma-off" mode of operation, the deformation behaviour of the alloy is likely to be modified. This kind of cyclic loading would induce not only fatigue damage but also make the material creep during the operation. Not much is known about the impact of this complicated mode of deformation on the mechanical performance of metals and alloys particularly in the environment of intense neutron irradiation.

In order to evaluate the effect of irradiation on the creep-fatigue behaviour, a number of CuCrZr specimens were irradiated with fission neutrons in the BR-2 reactor at Mol (Belgium). Specimens were irradiated to a displacement dose level of 0.2 – 0.3 dpa at 60 and 300^{o}C at a damage rate of ~4 – 5 x 10^{-8} dpa/s.

Both prime aged (PA) and over-aged (at 60^{o}C for 1 h) specimens of CuCrZr alloy were fatigue tested at room temperature in the irradiated and unirradiated conditions. Mechanicaltesting was carried out in an Instron machine with a servo-electrical mechanical test stand.

The loading cycles were always fully reversed (i.e. R = -1) so that the maximum tension load was the same as the maximum compressive load. The loading frequency was typically 0.25 Hz. Tests were conducted with tension and compression hold time of 0, 10 and 100 s. The specimen were cycled to failure.

Figure 5 shows the variation of number of cycles to failure (N_f) with stress-amplitude at room temperature for the prime aged CuCrZr alloy tested both in irradiated and unirradiated conditions. The results are shown for zero, 10 and 100 s holdtime both in tension and compression. In the unirradiated condition the holdtime of 100 s clearly reduces the number of cycles to failure compared to the results for the zero and 10 s holdtime. There is no clear difference between the results for the zero and 10 s holdtime. However, more results are needed to confirm this indication.

The effect of neutron irradiation on the number of cycles to failure (at a given stress amplitude) is very clear, in that the irradiated specimens show longer lifetime than the corresponding unirradiated specimens. The number of cycles to failure decreases with increasing holdtime but the decrease is not as large as in the case of unirradiated specimens. The difference in behaviour between the irradiated and unirradiated specimens may arise from the fact that the as-irradiated specimens are considerably stronger than the unirradiated specimens.

[6] TW2 – TVM – CUCFA and TW3 – TVM - CUCFAZ

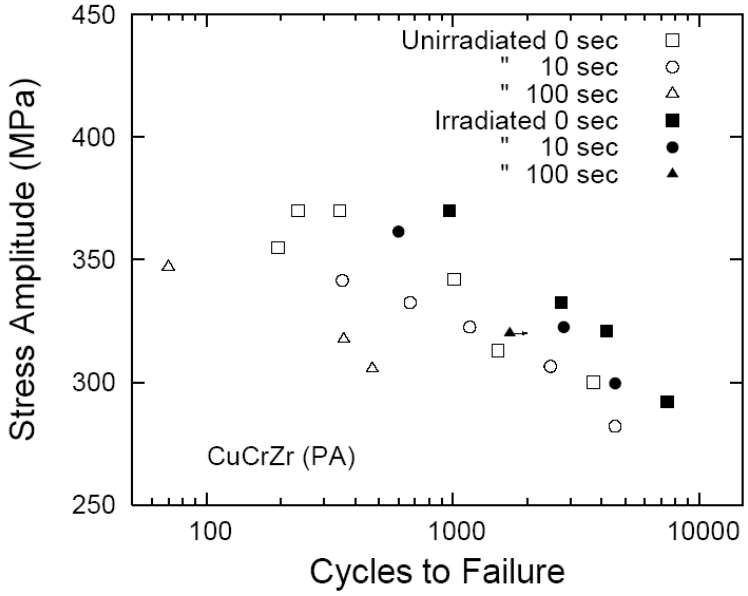

Figure 5.Number of cycles to failure (N_f) as a function of stress amplitude for CuCrZr alloy fatigue tested at room temperature with no holdtime and a tension and compression holdtime of 0, 10 and 100 seconds in the unirradiated and neutron irradiated conditions.

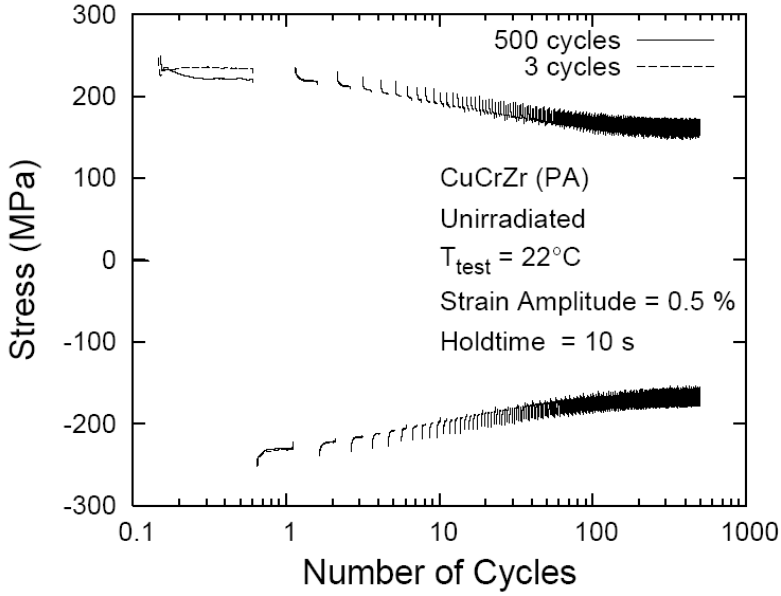

Figure 6. Number of cycles as a function of stress amplitude in "interrupted" creep-fatigue tests at room temperature carried out with a tension and compression holdtime of 10s. A number of specimens of unirradiated CuCrZr (PA) alloy were tested for 1, 2, 5, 25, 100 and 500 cycles. In these interrupted tests, the test was stopped after the given number of cycles (e.g. 1, 2, 5, 25, 100 and 500) and the surface of the deformed specimen was examined in a scanning electron microscope (SEM).

In addition to the regular creep-fatigue tests to failure, a number of "interrupted" creep-fatigue tests were performed on the prime aged CuCrZr alloy at room temperature with a holdtime of 10 s. In these tests, a number of specimens were given a pre-determined number of cycles. After a given number of cycles the specimen was unloaded for the microstructural examination. The surfaces of the deformed specimens were investigated for the appearance of slip steps as a function of the number of creep-fatigue cycles. Figure 6 shows that the magnitude of stress relaxation increases with increasing number of cycles. Figure 7 shows the

SEM micrographs showing the evolution of slip steps on the surface of the deformed specimens to 1, 25 and 500 cycles. As can be seen in Figure 7a, the slip steps appear already at the end of the first cycle. The number of slip steps increases with increasing number of cycles. Already at 500 cycles, a well defined crack can be seen at the surface (Fig. 7c). At this strain amplitude of 0.5%, the specimen fractures after about 3000 cycles.

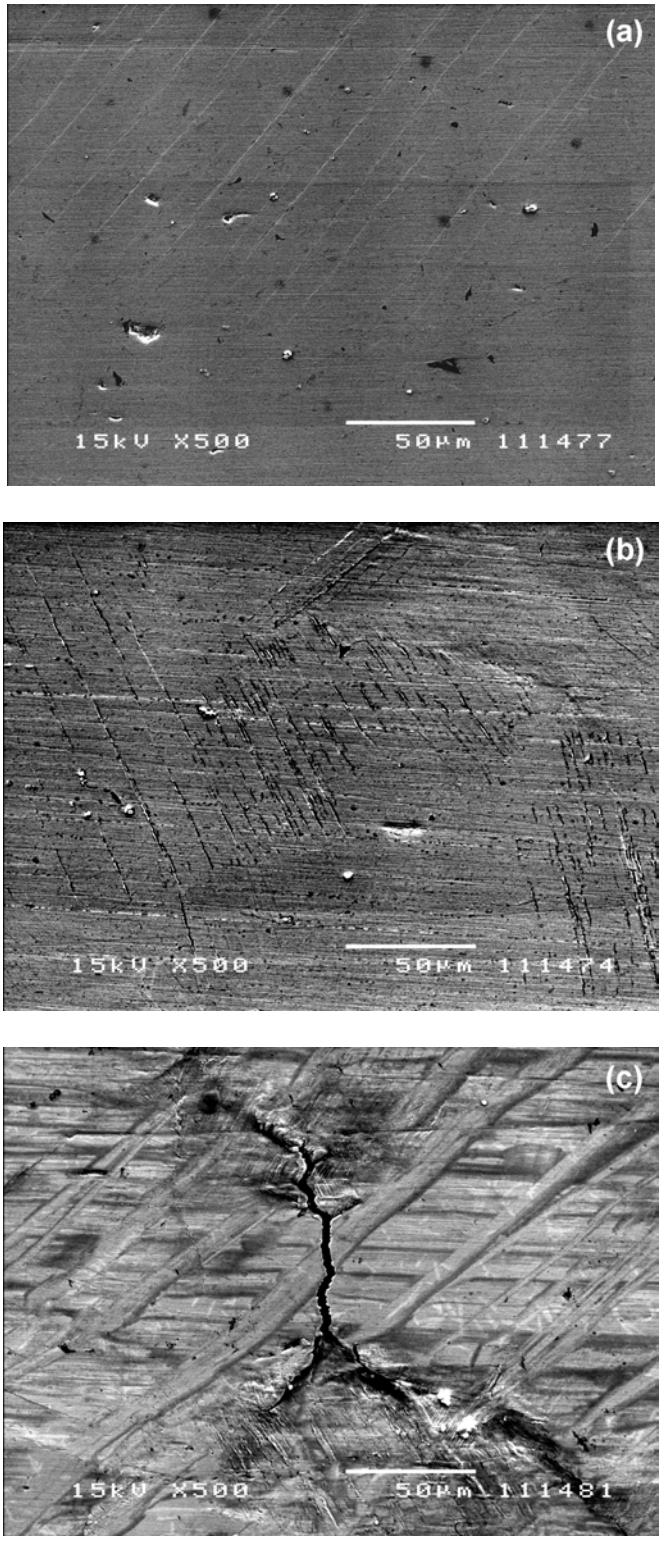

Figure 7. Scanning electron microscope (SEM) images showing slip steps at the surface of the specimens tested (in the interrupted tests) to different number of cycles: (a) 1, (b) 25 and (c) 500 cycles. Note that the slip steps appear already after the first cycle and the number increases with increasing number of cycles. At 500 cycles clearly visible crack can be seen in Fig. 7(c).

These results suggest that during creep-fatigue loading, plastic deformation becomes localized during very early stages of the test. This kind of deformation localization, for instance, at grain boundaries could easily lead to crack initiation at the boundaries. The growth of these crack may then cause fracture of the specimen.

3.2.3 Irradiation testing of as-fabricated CuCrZr/316 ss joints[7]

B.N. Singh, B.S. Johansen and S. Tähtinen (*VTT Industrial Systems (Association EURATOM-TEKES), Espoo, Finland)*

The current design of the International Thermonuclear Experimental Reactor (ITER) utilises copper alloys in the first wall module and divertor cassette components. At present CuCrZr alloy is being considered as the main candidate material for its use both in the first wall and the divertor components. The hot isostatic pressing (HIP) has been accepted as the appropriate technique for bonding the CuCrZr alloy to stainless steel. There is, however, very little known at present about the effect of neutron irradiation on the mechanical behaviour of such joints produced by the HIPing CuCrZr alloy and stainless steel. It was therefore, decided to investigate the effect of neutron irradiation on the tensile and fracture toughness behaviour of the as-fabricated CuCrZr/316 stainless steel joints. In the following, the results on tensile properties are reported. The corresponding results on the fracture toughness behaviour will be reported by the VTT Industrial Systems.

Tensile specimens of the as-fabricated CuCrZr/316 L(N) stainless steel joint were irradiated in BR-2 reactor at Mol (Belgium) at 60 and 300°C to a dose level of ~0.3 dpa. Prior to irradiation some of the specimens were given a heat treatment at 600°C for 4 hours. For comparison the base CuCrZr alloy specimens were also irradiated and tested in the prime aged (PA and annealed at 600°C for 4 h) condition. Post-irradiation tests were carried out at the irradiation temperature (i.e. 60 and 300°C). Both unirradiated and irradiated specimens were tested at a strain rate of 1.3 x 10^{-3} $s^{-1.}$

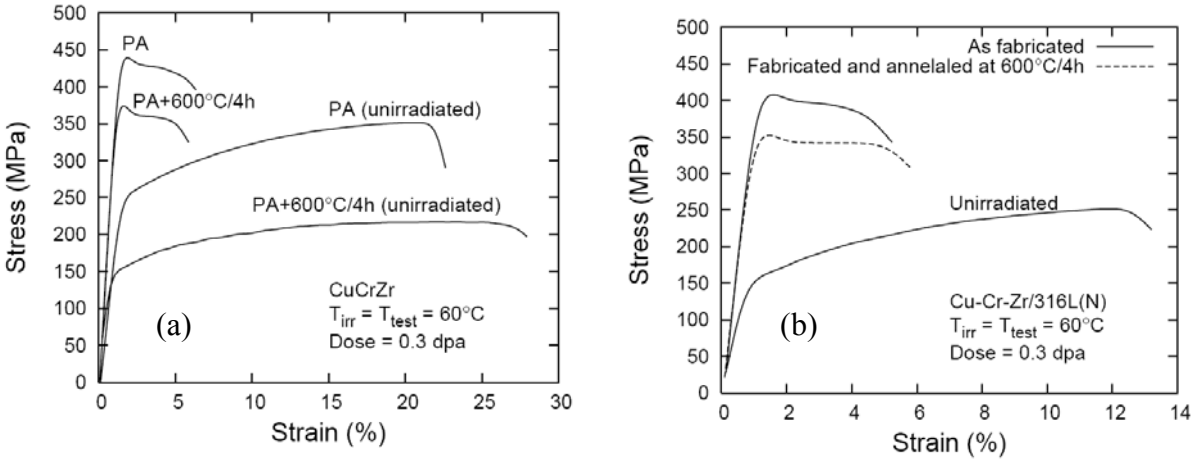

Figure 8. Stress-stress curves for (a) CuCrZr/316L(N) joint specimens and (b) the base CuCrZr alloy irradiated at 60°C to 0.3 dpa and tested at 60°C.

Figure 8(a) shows the stress-strain curves for the as-fabricated joint specimens irradiated and tested at 60°C. The stress-strain curves for the unirradiated (as fabricated) joint specimen is also shown in Figure 8(a). Figure 8(b) shows the stress-strain curves for the base CuCrZr alloy irradiated and tested at 60°C. The comparison of results in Figure 8(a) and 8(b) suggests

[7] Task TWO-T507/6

that the tensile behaviour of CuCrZr/316 L(N) joint specimens is very similar to that of the base CuCrZr alloy.

The stress/strain curves for the joint specimens irradiated (in the as fabricated and fabricated and annealed at 600°C for 4 h) and tested at 300°C are shown in Figure 9(a). Results demonstrate that irradiation at 300°C to a dose level of 0.3 dpa has practically no effect on the tensile behaviour of the as-fabricated joint specimens. The base CuCrZr specimens irradiated and tested at 300°C show, on the other hand, a clear sign of softening due to irradiation (Figure 9(b)).

It should be mentioned that both at 60 and 300°C, tested in both unirradiated and irradiated condition, all joint specimens fractured on the CuCrZr side of the joints.

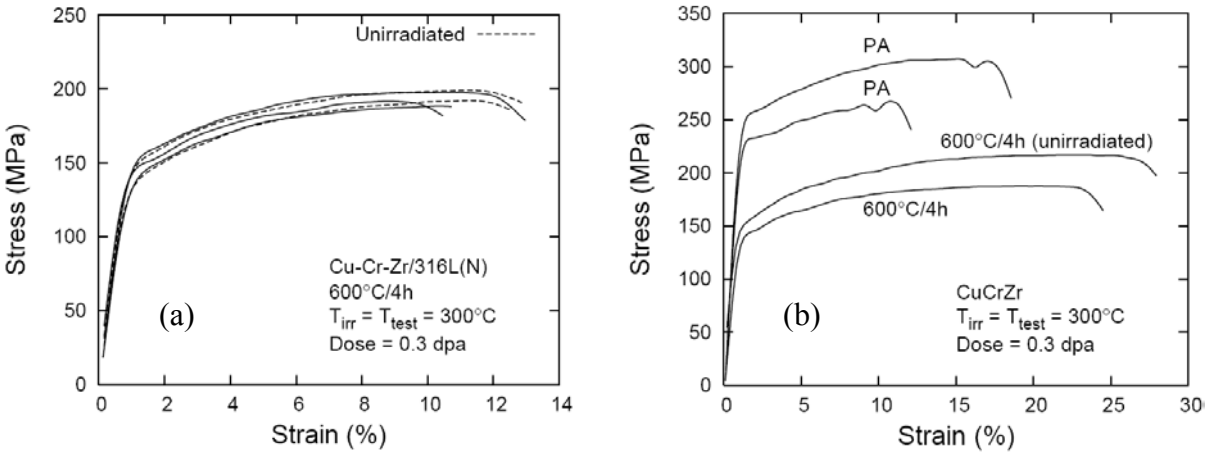

Figure 9. Stress-strain curves for (a) CuCrZr/316L(N) joint specimens and (b) the base CuCrZr alloy irradiated at 300°C to 0.3 dpa and tested at 300°C.

3.3 Long-term technology

3.3.1 Effect of helium implantation and neutron irradiation on tensile properties of iron and Eurofer-97 steel[8]

B.N. Singh, B.S. Johansen and P. Jung (*Association EURATOM-Forschungszentrum Jülich, Jülich, Germany)*

Effects of neutron irradiation on physical and mechanical properties of low activation ferritic-martensitic steels are being extensively studied internationally since these alloys are considered to be candidate materials for the blanket and first wall of fusion reactors (e.g. DEMO). Since fusion (14MeV) neutrons would generate a considerable amount of helium, the effect of helium on low temperature mechanical properties is a matter of concern. In order to simulate the effect of helium, various amount (1, 10 and 100 appm) of helium was implanted in pure iron and Eurofer-97 steel at temperatures below and above the recovery stage V (i.e. 50 and 350°C). In order to ensure a homogeneous distribution of the implanted helium, the thickness of specimens was chosen to be 100μm.

The helium implanted specimens were subsequently irradiated with fission neutron in the BR-2 reactor at Mol at a damage rate of 4.5 x 10^{-8} dpa/s to various dose levels in the range of 0.001 to 0.23 dpa at 60 and 350°C. The irradiated specimens were tensile tested at the implantation temperatures with a strain rate of 1.3 x 10^{-3} s^{-1}. For comparison purposes, some

[8] Task TTMS-001

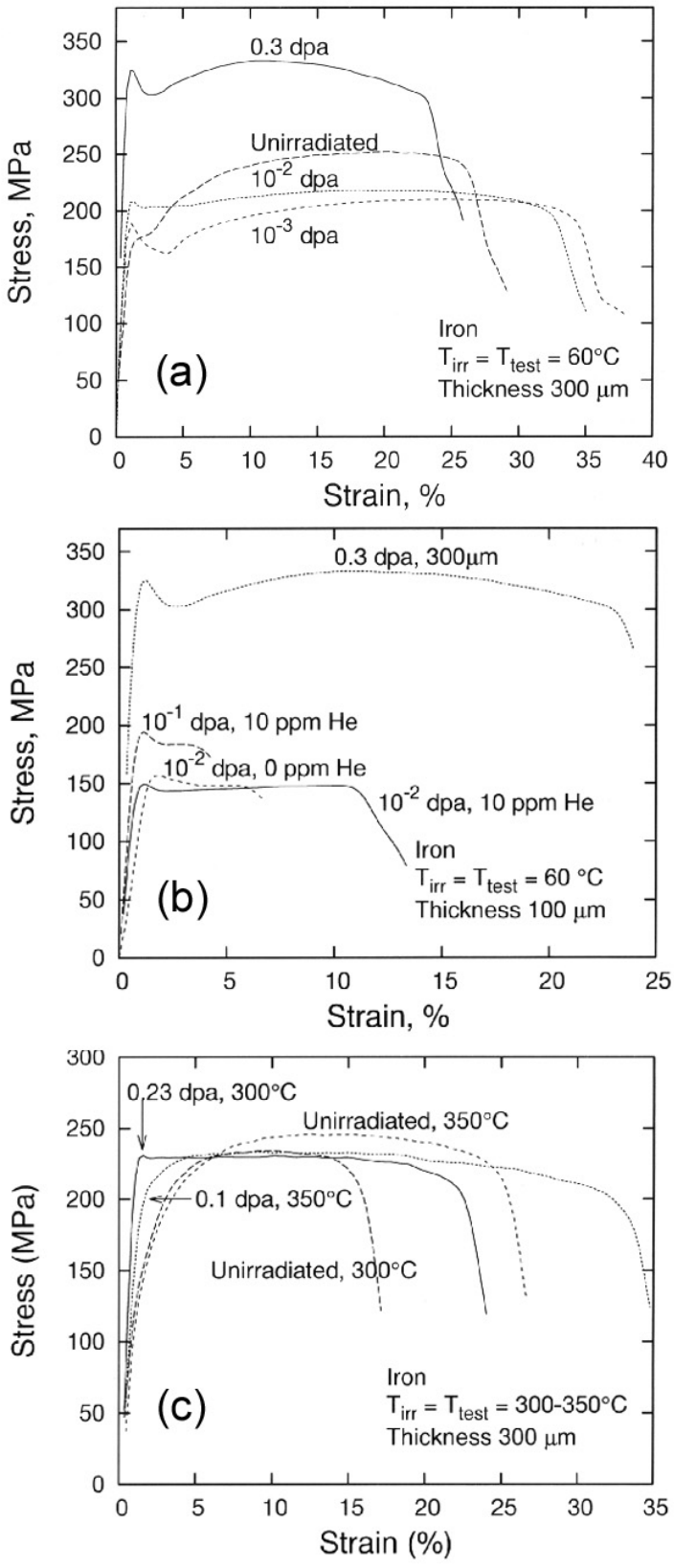

Figure 10. Stress-strain curves for pure iron with and without implanted helium and subsequently neutron irradiated at 60°C (Fig. 10a and 10b) and 300 – 350°C (Fig. 10c) to different displacement dose levels. Note the effect of specimen thickness and that the irradiation at 300 – 350°C does not seem to have any significant effect.

additional specimens of the standard thickness (i.e. 300 μm) were also irradiated and tensile tested exactly under the same conditions as the implanted specimens. Some examples of the stress-strain curves obtained at 50 and 350°C are shown in Figures 10 and 11, respectively. The unimplanted specimens of the standard thickness (i.e. 300 μm) exhibit the expected effect of irradiation both at 60 and 350°C in that (a) at 60°C the yield strength increases and elongation decreases due to irradiation and (b) at 350°C, the effect of irradiation on mechanical properties is very small. In the case of helium implanted specimens, on the other hand, the results do not appear to be consistent and reliable. This is, in all probability, simply because the helium implanted specimens are too thin for mechanical testing. In other words, as regards the effect of helium and neutron irradiation on the mechanical performance of iron and Eurofer-97, no reliable conclusion can be drawn from the present results.

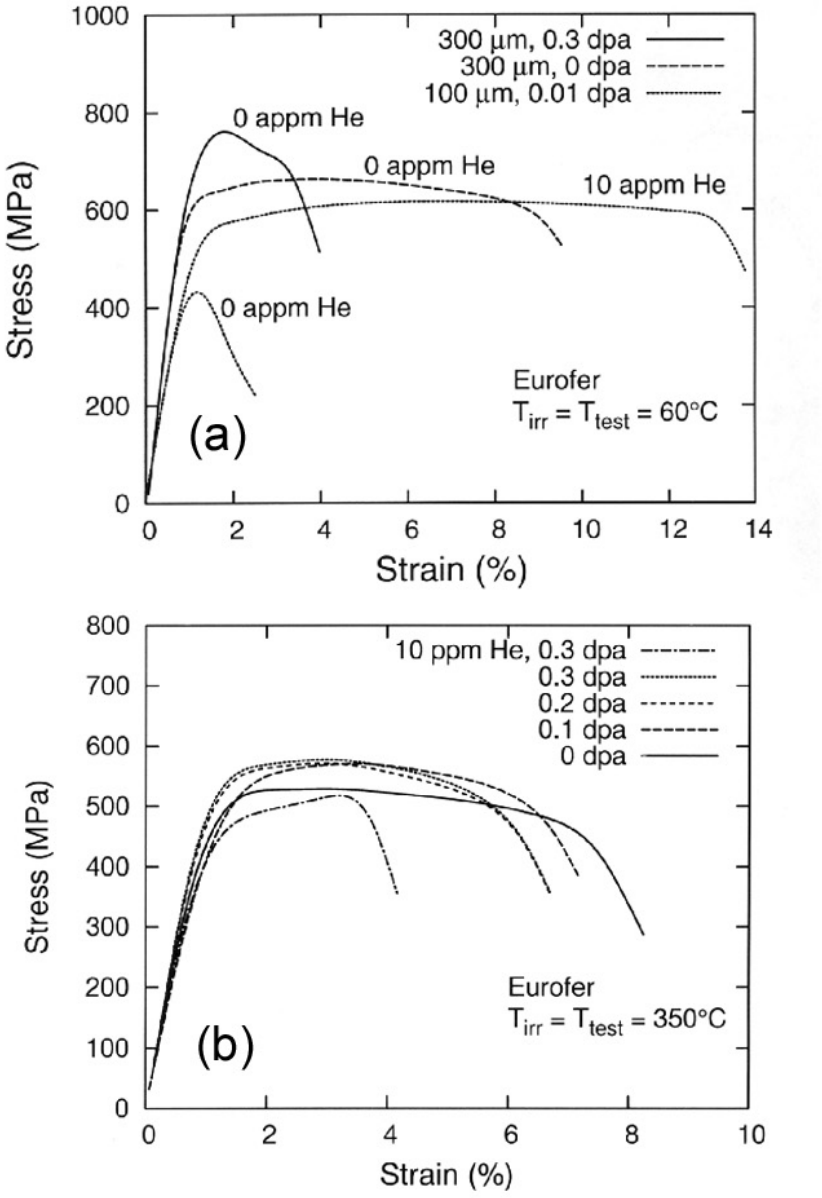

Figure 11. Stress-strain curves for Eurofer-97 with and without implanted helium and subsequently neutron irradiated at 60°C (Fig. 11a) and at 350°C (Fig. 11b).

3.3.2 Effect of helium implantation and neutron irradiation on cavity formation in iron and Eurofer-97

M. Eldrup, B. N. Singh, P. Jung (*Association EURATOM-Forschungszentrum Jülich, Jülich, Germany) and D. J. Edwards** (** Pacific Northwest National Laboratory, Richland, USA)*

As mentioned in section 3.3.1 above, neutron irradiation effects on low activation steels, which are candidate materials for fusion reactors, are being studied extensively. As part of this effort, Positron Annihilation Spectroscopy (PAS, which is sensitive to cavities in the size range from single vacancies to several nano-metres) and TEM investigations have been carried out on the effect of helium implantation and neutron irradiation on cavity formation in pure iron and Eurofer-97. The specimens used for this study were prepared in the same way as the ones described in section 3.3.1.

As discussed earlier (Annual Report 2002), PAS results show that like in the case of neutron irradiation, nano-cavities are formed during He implantation both in pure Fe and in Eurofer-97 at 50°C and at 350°C. Figure 12 illustrates some of the effects of neutron irradiation after He implantation, which have been observed. For all cases of implanted and/or neutron irradiated iron or steel, long-lived components in the positron lifetime spectra give evidence of the presence of small cavities in the specimens.

In Eurofer-97, a clear effect of neutron irradiation (0.01dpa) after He implantation (100 ppm He) is observed at 50°C (Fig. 12a). However, the results for neutron irradiated specimens with or without prior He implantation are very similar. Hence, the effect of He on the microstructure as detected by PAS after neutron irradiation is rather small. At 350°C, neutron irradiation after He implantation gives rise to only a small change in the data (Fig. 12b), while in iron at 350°C the effect of irradiation is bigger (Fig. 12c). Again the data show a rather small effect of the presence of He on the results for neutron irradiated specimens.

A more detailed, quantitative analysis of the PAS data is in progress. As an example, the densities of cavities can be derived from the data in Fig. 12c for iron, which has been He implanted and/or neutron irradiated at 350°C. After neutron irradiation to a dose of 0.23 dpa the density of small voids is ~ 10^{22} m^{-3}, while the He bubble density after implantation of 100 ppm He is estimated to be appreciably higher, i.e. about 5×10^{23} m^{-3}. For the case of neutron irradiation (0.1dpa) after implantation with 100 ppm He, the He bubble density in iron is estimated to be~5×10^{21} m^{-3}, in fair agreement with the findings by TEM (see below). In this case, the helium density inside the bubbles as estimated from the positron lifetime is found to be 2.1×10^{28} m^{-3}, in agreement with the TEM estimate of 1.9×10^{28} m^{-3}.

For the TEM examinations, foils of pure iron and Eurofer-97, that were prepared in the same way as the ones described in section 3.3.1, were used. Specimens implanted with He at 50°C and neutron irradiated at 50°C showed the presence of only black dot damage (i.e. very small interstitial or vacancy loops). No visible cavities could be resolved in these specimens. Specimens of pure iron helium implanted (100 ppm) at 350°C and neutron irradiated also at 350°C to a dose of 0.23 dpa did show the presence of a modest density of resolvable loops (most probably of interstitial type) and a high density (~ 10^{22} m^{-3}) of rather small (~ 3.5 nm) cavities. An example of both loop and cavity microstructure is shown in Fig. 13. Cavities were also observed in Eurofer-97 implanted with 100 ppm helium and neutron irradiated at 350°C (Fig. 14). The cavity distribution in the Eurofer-97 was found to be very heterogeneous whereas in pure iron, the cavities were found to be distributed rather homogeneously.

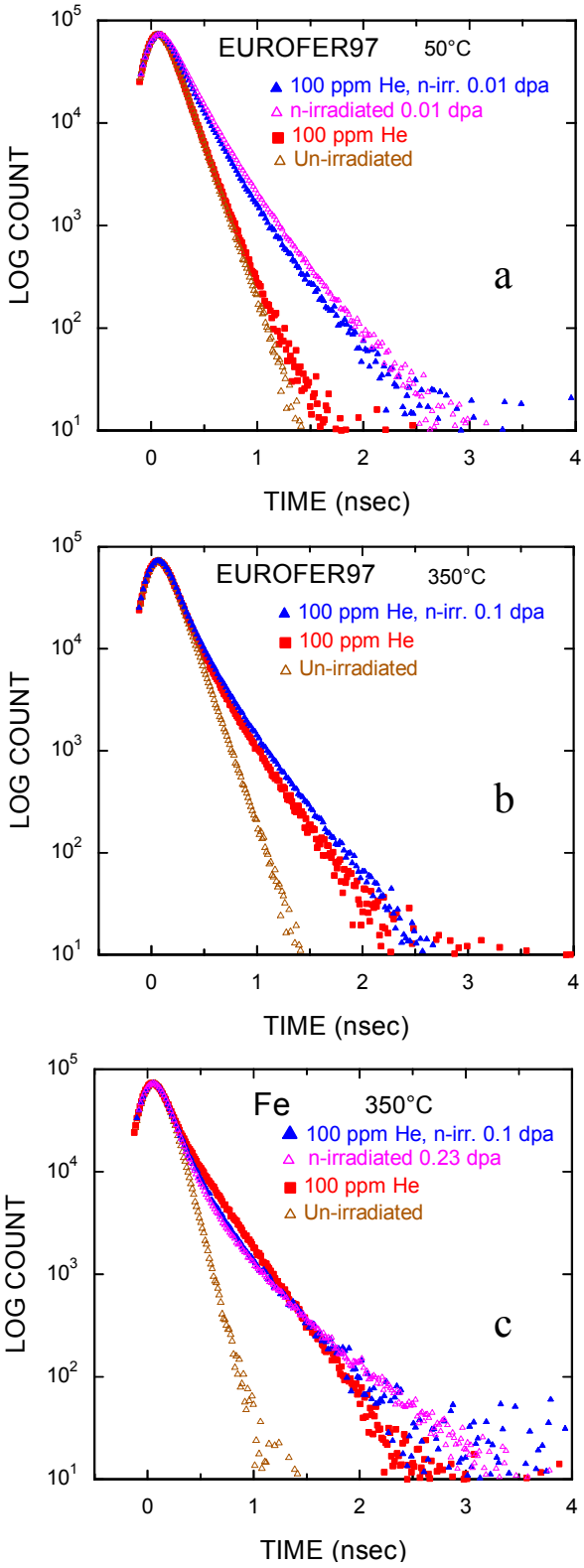

Figure 12. Comparison of positron lifetime spectra for He-implanted and /or neutron irradiated pure iron and Eurofer-97. In fig. a), a clear effect of neutron irradiation (0.01dpa) after He implantation (100 ppm He) is observed in Eurofer-97 at 50°C. The results for neutron irradiated specimens with or without prior He implantation are very similar, i.e. the effect of He on the microstructure as detected by PAS after neutron irradiation is rather small. At 350°C (fig. b), neutron irradiation after He implantation gives rise to only a small change in the data. In iron at 350°C the effect of irradiation is bigger (fig. c), but the results for neutron irradiated specimens seem only slightly influenced by pre-implanted He.

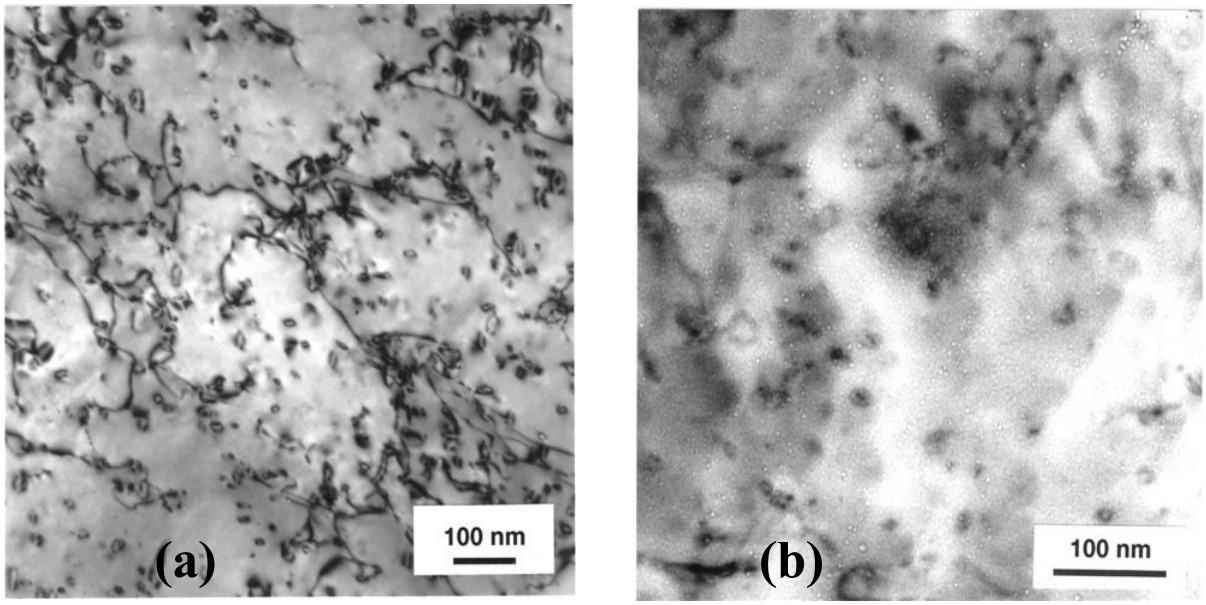

Figure 13. Transmission electron micrographs for pure iron implanted with 100 appm of helium at 350°C and subsequently neutron irradiated at 350°C to a dose level of 0.3 dpa showing: (a) loops and dislocations and (b) cavities. Note that the cavities are formed in a homogeneous manner.

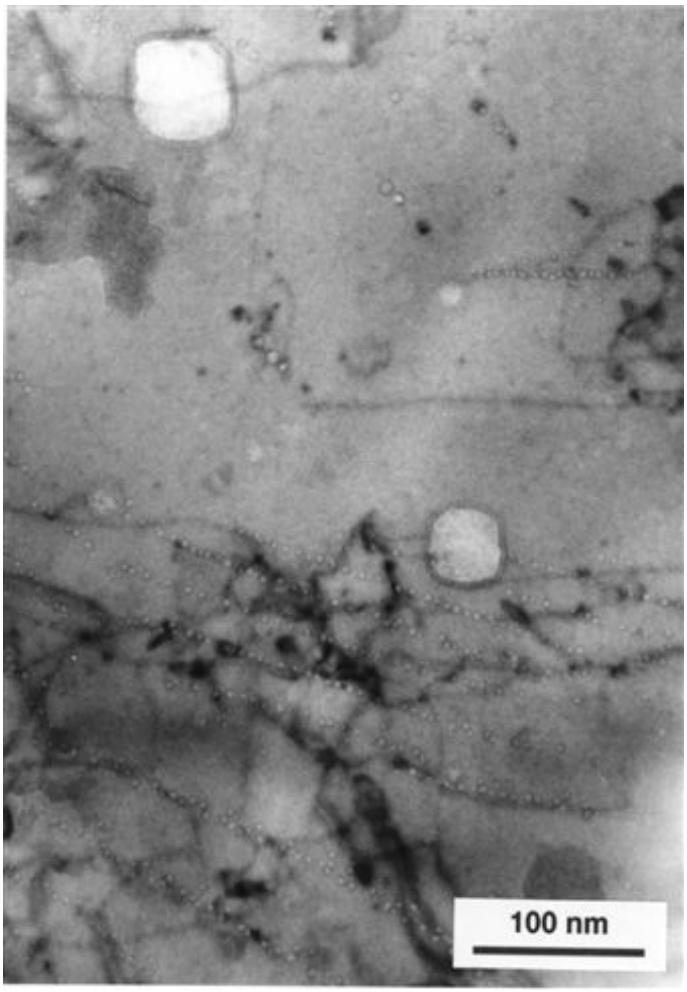

Figure 14. The same as in Fig. 13 but for the Eurofer-97 steel. The distribution of cavities is very heterogeneous and they appear to form only on dislocations and interfaces.

3.3.3 Modelling of cavity evolution in bcc iron and steels with and without helium[9]

B.N. Singh, S.I. Golubov (*Oak Ridge National Laboratory, Oak Ridge, USA) and M. Eldrup*

The problem of void swelling at elevated temperatures is a matter of concern for structural materials employed particularly in the environment of 14 MeV neutrons in a fusion reactor. The 14 MeV neutrons not only produce displacement cascades, they also generate helium atoms via nuclear reaction at a relatively high rate. The kinetics of defect accumulation under these conditions is very complicated and is not well understood, particularly in the bcc crystal structure. We have demonstrated experimentally that during neutron irradiations voids are formed both in pure iron and ferritic steels (F82H and Eurofer-97) already at the irradiation temperatures of 50 – 100°C. Implantations of helium at 50°C also produces a high density of cavities. After these observations, a systematic investigation of the effect of helium on cavity nucleation and growth in pure iron and Eurofer-97 was initiated. Some results were reported already last year and new results obtained recently are reported in section 3.3.2.

One of the objectives of the experimental investigations was to generate sufficient experimental results to validate the predictions of analytical and/or numerical calculations of the effect of helium on cavity nucleation and growth. Recently, we have initiated a detailed numerical calculation of the kinetics of cavity nucleation and growth under cascade damage conditions. The computer code developed earlier to treat the problem of void swelling within the framework of the production bias model has been modified to include the treatment of helium implantation/generation. The problem is treated within the framework of the production bias model. Two dimensional kinetic equation for size distribution function of helium-vacancy clusters is used to describe the cluster evolution in the case of helium-ion irradiation. A new grouping method has been developed to solve the kinetic equation for the size distribution functions of point defect clusters.

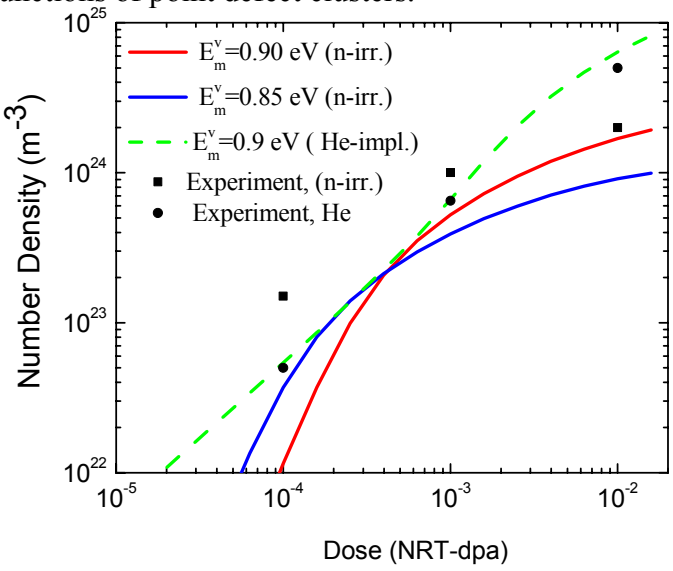

Figure 15. Dose dependence of cavity density calculated for pure iron irradiated at 50°C with neutrons (solid lines) and helium ions (broken lines). For comparison, experimental results for both types of irradiations are also shown.

Some of the preliminary results of these calculations are shown in Figs. 15 and 16. Fig. 15 shows a qualitative comparison of the experimental measured and the calculated dose dependence of cavity density. In the case of neutron irradiation, the calculations have been performed for several different values of vacancy migration energy since no reliable value for

[9] Task TTMS-001.

the migration energy is known from experiments. As can be seen in Fig. 15, the results obtained with the energy of 0.9 eV are in reasonable agreement with the experimental results at doses larger than 10^{-3} dpa. The size distributions of cavity for a terminal dose of 1.5 x 10^{-2} dpa is shown in Fig. 16. These results are also consistent with experimental results.

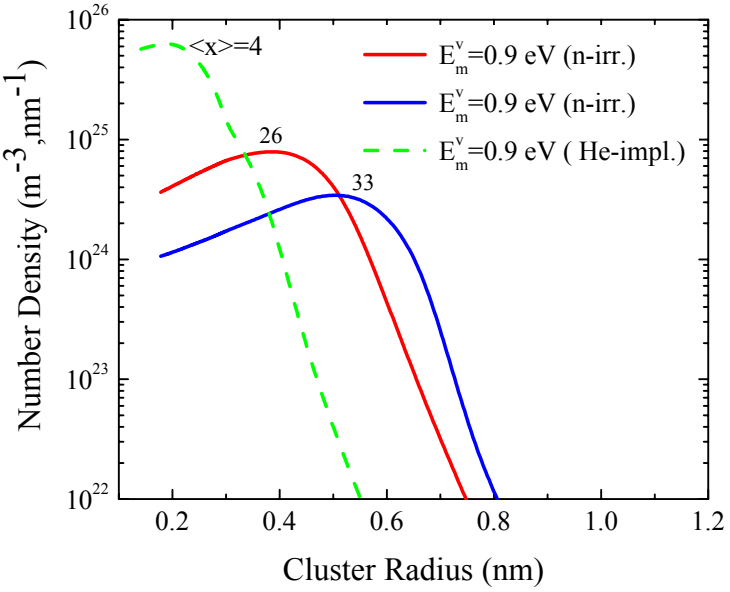

Figure 16. Size distribution functions of cavities for a terminal dose of 1.5 x 10^{-2} dpa calculated for the cases of neutron and helium ion irradiations shown in Fig. 15. <x> is the number of vacancies accumulated in the cavities at the peak densities.

3.4 Underlying technology

3.4.1 1-D to 3-D diffusion reaction kinetics of SIA clusters – implications for the evolution of voids

H. Trinkaus (*Association EURATOM-Forschungszentrum Jülich, Jülich, Germany), B.N. Singh and S.I. Golubov** (**Oak Ridge National Laboratory, Oak Ridge, USA)*

In pure metals subject to cascade damage generating irradiation such as fusion neutron irradiation, damage accumulation at low doses (<1 dpa) and medium temperature occurs in a pronounced segregated fashion: self-interstitial atoms (SIAs) segregate in the form of dislocation loops near dislocations or form rafts of loops (at temperatures between 0.2 and 0.4 T_m). At high doses (> 1 dpa), in some metals, voids cease growing and, in many metals, they order in the form of void super-lattices. These phenomena do not only depend on the irradiation parameters, but also on the crystal and micro-structure as well as the composition of the metal, in particular on the concentration of impurities which generally tend to extinguish the phenomena.

In the last decade, these phenomena have been rationalized in terms of intra-cascade clustering of vacancies as well as self-interstitial atoms (SIAs), differences in the thermal stability and mobility of the resulting clusters and one-dimensional (1-D) diffusion of SIA clusters in the form of small dislocation loops. Their dependence on the material state and irradiation parameters remained, however, unclear. The 1-D diffusion of SIA clusters is generally disturbed by two different types of processes: change of the diffusion direction

between equivalent crystal directions and transversal diffusion due to self-climb, both resulting in diffusion reaction kinetics between the 1-D and 3-D limiting cases.

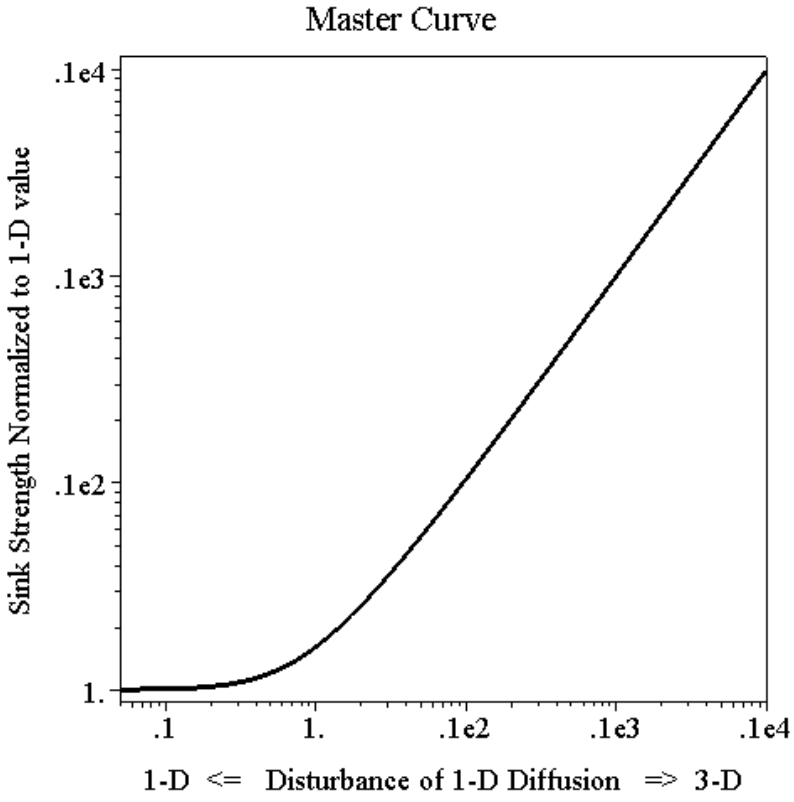

Figure 17. Sink strength normalised to its value for pure 1-D, $k^2/k_{(1)}^2$, vs measure for the "disturbance of 1-D diffusion". The meaning of "disturbance of 1-D diffusion" is $(l^2k_{(1)}^2/4+k_{(1)}^4/k_{(3)}^4)^{-1/2}$ and $(\delta^{1/2}k_{(3)}^2/k_{(1)}^2$ for disturbance by direction changes and transversal diffusion, respectively (l: mean 1-D diffusion length, $\delta = D_{tr}/D_{lo}$ ratio of transversal to longitudinal diffusivity).

For the disturbance by direction changes, we have derived an analytical single-variable function (“master curve”) interpolating between the 1-D and 3-D limiting cases, in excellent agreement with kinetic Monte Carlo simulations (Phys. Rev. B. 66, 060105®, 2002). For the disturbance of 1-D diffusion by transversal diffusion, we have recently shown that the kinetics can be described by a master curve of the same form as for the disturbance by direction changes if the variable for the effective disturbance of 1-D diffusion is chosen properly (see Fig. 17). In both cases, this variable does not only contain the disturbance itself but also the parameters characterising the sink structure (density and size expressed by 1-D and 3-d sink strengths). The sink strength for the absorption of SIA clusters increases continuously with increasing effective 1-D disturbance from very low values for the 1-D to high values for the 1-D to high values for the 3-D limiting case.’

We have applied our analytical theory of 1-D to 3-D diffusion reaction kinetics to the saturation of void growth at high doses. It is found that the saturation size increases continuously with increasing effective disturbance of 1-D diffusion. In the case of disturbance by direction changes, the increase becomes significant only when the kinetics comes relatively close to the 3-D limiting case. In the case of disturbance by transversal diffusion, the increase is much more continuous depending on the dislocation and void densities as shown in Fig. 18. Figure 18 suggests that differences in the observed high dose evolution of voids between bcc (Mo) and fcc metals (Cu), i.e. observation or missing observation of void growth saturation (and void lattice formation), respectively, is simply due to the much higher void densities in the former than in the latter case (2 orders of magnitude difference). This interpretation would

further imply that the disturbance of 1-D diffusion of SIA clusters (loops) at void formation temperatures is mainly due to transversal diffusion by self-climb.

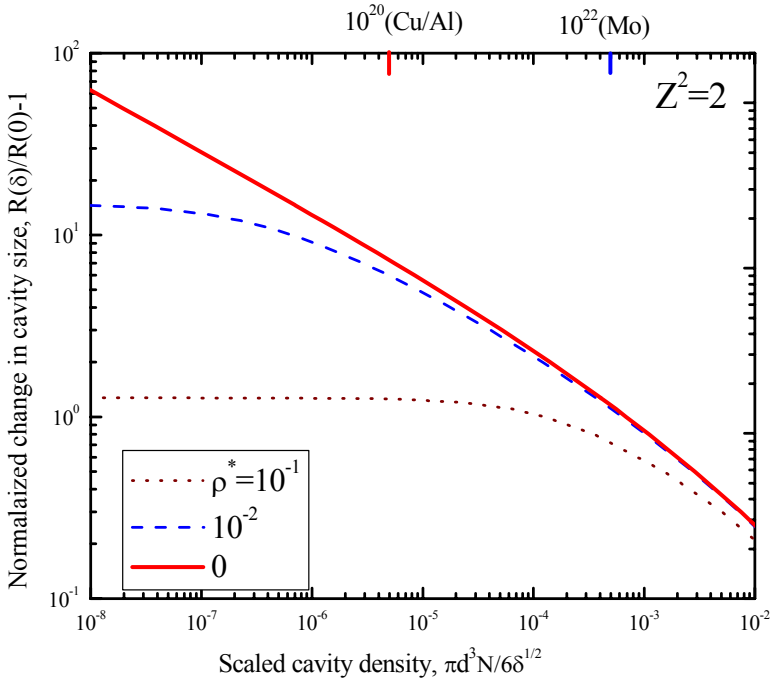

Figure 18. Change in saturation size of cavities due to transversal diffusion normalized to value for vanishing transversal diffusion, *R(δ)/R(0)*-1, vs scaled cavity density for different values of scaled dislocation density, $\rho^*(\delta = D_{tr}/D_{lo})$ ratio of transversal to longitudinal diffusivity, *d*: cluster absorption diameter of dislocations, *Z*: cluster dislocation bias, *N*: cavity density). Typical values of scaled cavity densities for fcc (Cu, Al) and bcc metals (Mo) are indicated. Note that the change in saturation size is moderate in the case of bcc but very significant in the case of fcc metals.

3.4.2 Kinetic Monte Carlo (KMC) simulation of segregation and accumulation of interstitial clusters during neutron irradiation of bcc iron

Ming Wen (*University of California Los Angeles, Los Angeles, USA),*
N.M. Ghoniem and B.N. Singh*

It is well known that during neutron irradiations at low temperatures (i.e. below the recovery stage V), the accumulation of interstitial clusters produced in the cascades occurs in a very segregated fashion. The segregation of interstitial loops in the form of decoration of grown-in dislocation and/or rafts of these loops is particularly prominent in bcc crystals since most of the interstitial clusters produced in the cascades are highly glissile. In the case of bcc iron, the situation gets further complicated because of the formation of nano-voids even at these temperatures. According to the cascade induced source hardening (CISH) model[10], this kind of segregation of the interstitial loops may be responsible for the observed decrease in ductility of neutron irradiated iron. At present, there exists no theoretical framework within which this problem of segregation and accumulation of interstitial clusters can be treated adequately. It was, therefore, decided to initiate a detailed and dynamic computer simulation of the whole evolution process.

In the present simulations, the defects generated by a number of 40 keV cascades corresponding to a damage rate of 5 x 10^{-8} dpa/s are introduced at the appropriate frequency in

[10] B.N. Singh, A.J.E. Foreman and H. Trinkaus, J. Nucl. Mater. 251 (1997) 103.

the simulation box (0.25 μm x 25 μm x 0.25 μm). The defect statistics for clusters are taken from the results of molecular dynamic (MD) simulations. The magnitude of 1-D diffusional glide of the interstitial clusters and the frequency of change in direction of these clusters are also taken from the results of MD simulations. Once the defect clusters are introduced their spatial and temporal evolution is followed by the KMC code. The present code incorporates the elastic interaction between various components of the evolving microstructure. As cluster density increases with increasing displacement dose level, the calculation of elastic interactions amongst all the clusters becomes very time consuming. Consequently, so far, the microstructural evolution has been calculated to doses of only up to 5.21 x 10^{-3} dpa

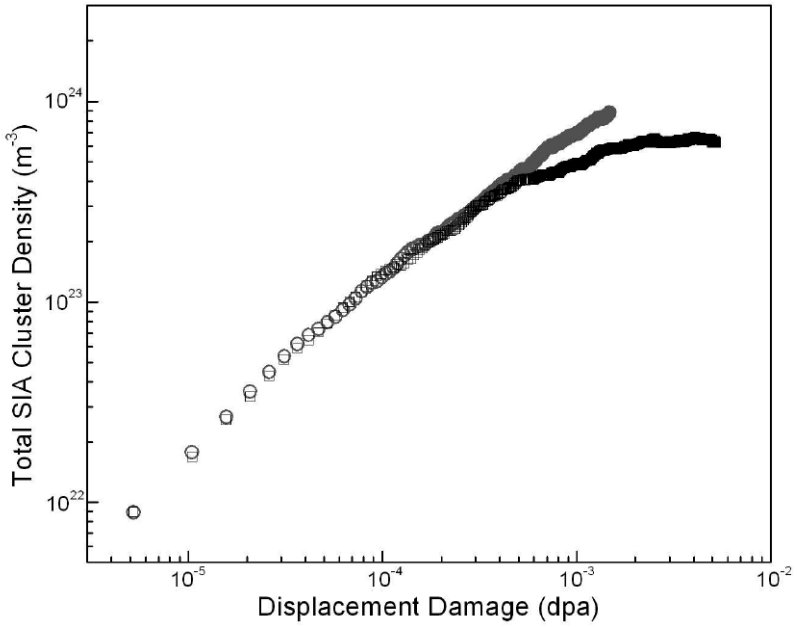

Figure 19. Dose dependence of the total SIA cluster density calculated for bcc iron corresponding to neutron irradiation at 27°C with (□) and without (O) the presence of nano-voids.

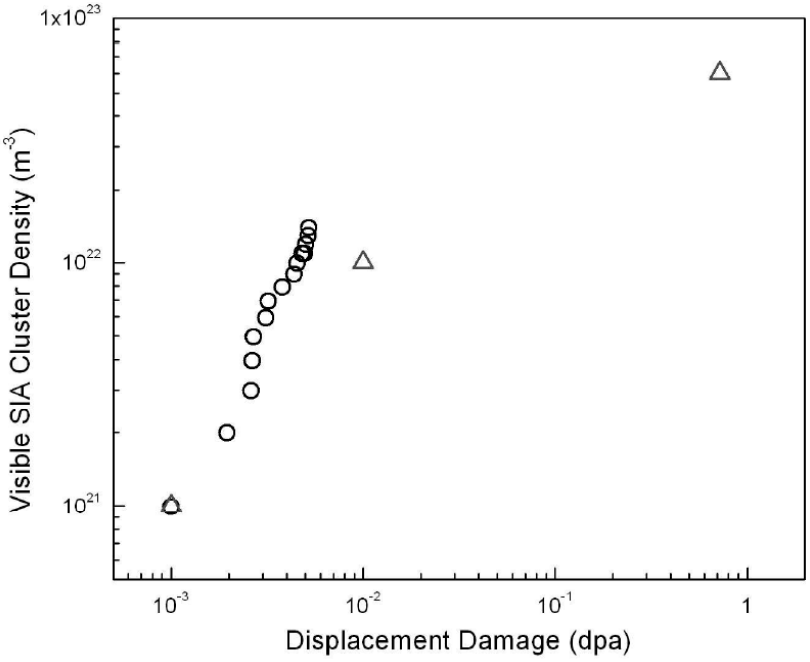

Figure 20. Dose dependence of visible SIA cluster density in bcc iron: O–KMC simulation results and Δ-experimental results for neutron irradiated at ~70°C.

The results show that the dislocation decoration builds up very quickly already at a dose level of 3 x 10^{-4} dpa and becomes very significant at a dose level of 1.3 x 10^{-3} dpa. The formation of rafts becomes evident at a dose level of 1.8 x 10^{-3} dpa. Figure 19 shows the dose dependence of the total cluster density with and without the recombination of interstitial clusters with nano-voids showing that the effect of recombination becomes significant above the dose level of ~5 x 10^{-4} dpa. In order to compare the calculated results with those obtained experimentally using electron microscopy, the dose dependence of the "visible" cluster density is shown in Fig. 20. Here, it is assumed that the clusters containing 100 interstitials become visible in the electron microscope. The general trend of the dose dependence of the cluster density calculated in the present work is qualitatively consistent with the experimental results.

3.4.3 Post-irradiation annealing of OFHC-copper irradiated at 250°C

B.N. Singh, M. Eldrup and D.J. Edwards (*Pacific Northwest National Laboratory, Richland, USA)*

It is well established experimentally that the primary damage production in copper under neutron irradiation is dominated by the formation of stacking fault tetrahedra (SFTs) in the cascade core. Since they are stable thermally as well as configurationally, their density increases very rapidly with dose and comes to saturate at very high concentration levels. Consequently, at all irradiation temperatures and particularly at temperatures below the recovery stage V, they become the dominating sinks for vacancies during irradiation. In other words, the kinetics of void nucleation and growth is strongly influenced by the sink strength of SFTs. In order to understand the details of void swelling behaviour as a function of irradition temperature, it is essential to understand the annealing kinetics of SFTs. Two series of annealing experiments have been carried out. The results of the one series of experiments were reported last year. In the following, some of the results of the second series are described.

A number of tensile specimens of OFHC-copper were irradiated in the DR-3 reactor at Risø at 250°C and at a damage rate of 5 x 10^{-8} dpa/s to a dose level of ~0.3 dpa. Irradiation was performed in an atmosphere of a mixture of helium and argon. For the present investigations, the irradiated specimens were annealed in vacuum at 300, 350, 400, 450 and 500°C for two hours. Both as-irradiated and annealed specimens were investigated using TEM and positron annihilation techniques. Some of the results obtained from TEM are described below.

Before describing the quantitative results it should be pointed out that irradiations at 250°C produces not only SFT_S but also a relatively dense population of voids. Both voids and SFTs are likely to emit vacancies at the annealing temperatures used in the present investigation. It is, therefore, expected that the annealing kinetics of SFT_S is likely to be complicated in the presence of voids since voids would also act as sinks for the vacancies emitted from SFT_S.

Figure 21 shows the size distributions of SFT_S determined from the TEM micrographs taken from the as-irradiated and post-irradiation annealed specimens. The mean size and average density of both SFT_S and voids are quoted in Table 1 for different annealing temperatures. Results quoted in Fig. 21, illustrate two clear effects of annealing: (a) increasing number of small SFT_S get annealed out with increasing annealing temperature and (b) for some reasons SFT_S are unable to grow in size beyond about 9 nm. Furthermore, it is also very clear that a significant number of larger SFT_S in fact grow in size during annealing. Both of these features demonstrate that the annealing kinetics is not being controlled by a simple

mechanism such as Oswald ripening. A detailed theoretical analysis will be carried out to determine the mechanism(s) controlling the annealing kinetics of SFT_S.

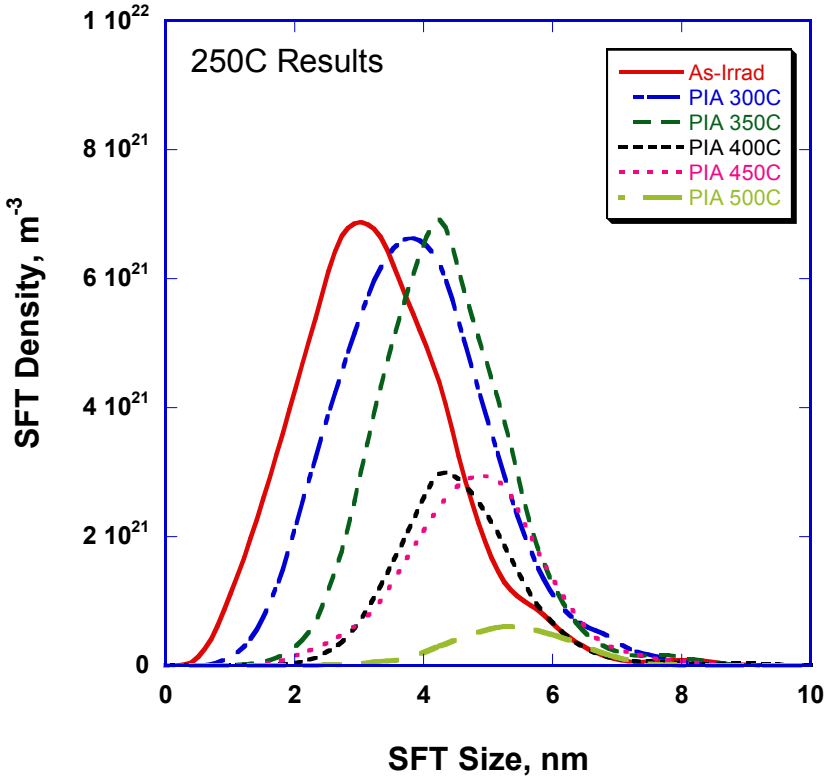

Figure 21. Size distributions of stacking fault tetrahedra (SFTs) for OFHC-copper irradiated at 250°C and subsequently annealed for 2 hours at 300, 350, 400, 450 and 500°C.

Table 1. Size and density of stacking fault tetrehedra (SFT_S) and voids in OFHC-copper irradiated at 250°C to 0.3 dpa and subsequently annealed at different temperatures (300, 350, 400, 450 and 500°C) for 2 hours.

Annealing Conditions	***Mean Size***		***Average Density***	
	Voids (nm)	***SFT_S (nm)***	***Voids (10^{20} m^{-3})***	***SFT_S (10^{22} m^{-3})***
As-irradiated	*15.1*	*3.30*	*3.5*	*4.0*
300°C/2 h	*16.2*	*3.85*	*5.0*	*3.9*
350°C/2 h	*15.7*	*4.30*	*4.9*	*4.2*
400°C/2 h	*15.3*	*4.50*	*5.1*	*1.3*
450°C/2 h	*17.0*	*4.80*	*<7.6*	*1.5*
500°C/2 h	*16.6*	*5.35*	*<2.8*	*0.28*

3.5 Publications and conference contributions

3.5.1 International publications

Edwards, D.J.; Singh, B.N.; Tähtinen, S.; Moilanen, P.; Jacquet, P.; Dekeyser, J., Status of in-reactor tensile straining of pure copper at a constant strain rate. In: Fusion materials. Semiannual progress report for the period ending June 30, 2003. DOE/ER-0313/34 (2003) p. 79-84

Edwards, D.J.; Singh, B.N.; Eldrup, M., The effect of post-irradiation annealing on stacking fault tetrahedra in neutron-irradiated ofhc copper. In: Fusion materials. Semiannual progress report for the period ending June 30, 2003. DOE/ER-0313/34 (2003) p. 85-92

Edwards, D.J.; Singh, B.N., Status of collaborative research program between PNNL and Risø National Laboratory. In: Fusion materials. Semiannual progress report for the period ending December 31, 2002. DOE/ER-0313/33 (2003) p. 111-119.

Eldrup, M.; Singh, B.N., Accumulation of point defects and their complexes in irradiated metals as studied by the use of positron annihilation spectroscopy - a brief review. J. Nucl.Mater. (2003) v. 323 p. 346-353.

Heinisch, H.L.; Singh, B.N., Kinetic Monte Carlo simulations of void lattice formation during irradiation. Phil. Mag. (2003) v. 83 p. 3661-3676

Heinisch, H.L.; Singh, B.N., Kinetic Monte Carlo simulations of the effects of 1-D defect transport on defect reaction kinetics and void lattice formation during irradiation. In: Fusion materials. Semiannual progress report for the period ending December 31, 2002. DOE/ER-0313/33 (2003) p. 146-150

Osetsky, Y.N.; Bacon, D.J.; Serra, A.; Singh, B.N.; Golubov, S.I., One-dimensional atomic transport by clusters of self-interstitial atoms in iron and copper. Phil. Mag. (2003) v. 83 p. 61-91

Singh, B.N.; Tähtinen, S.; Moilanen, P.; Jacquet, P.; Dekeyser, J., In-reactor uniaxial tensile testing of pure copper at a constant strain rate at 90 deg. C. J. Nucl. Mater. (2003) v. 320 p. 299-304

Trinkaus, H.; Singh, B.N., Helium accumulation in metals during irradiation - where do we stand?. J. Nucl.Mater. (2003) v. 323 p. 229-242.

3.5.2 Danish reports

Bindslev, H.; Singh, B.N (eds.), Association Euratom - Risø National Laboratory annual progress report 2002. Risø-R-1414(EN) (2003) 53 p.

Singh, B.N, Final report for the year 2001 on experimental and theoretical investigations of irradiation effects on physical and mechanical properties of iron and RAFM steels. Risø-R-1422(EN) (2003) 28 p.

3.5.3 Unpublished conference contributions and lectures

Edwards, D.J.; Singh, B.N., Evolution of cleaned channels in neutron-irradiated pure copper as a function of strain. 11. International conference on fusion reactor materials (ICFRM-11), Kyoto (JP), 7-12 Dec 2003. Unpublished.

Eldrup, M.; Singh, B.N.; Jung, P., A comparison of helium implanted iron and EURO-FER97: Effects of He dose. TMS 2003 annual meeting: Symposium on microstructural processes in irradiated materials, San Diego (US), 3-6 Mar 2003. Unpublished. Abstract available

Eldrup, M., Examples of detection and characterisation of defects in metals by positron annihilation spectroscopy. National Institute for Materials Science, Tsukuba, Japan, 5 Sep. 2003. Unpublished.

Eldrup, M.; Singh, B.N.; Edwards, D.J.; Nagai Y.; Ohkubo, H.; Hasegawa, M., Neutron irradiated copper: Is the main positron lifetime due to Stacking Fault Tetrahedra? 13'th International Conference on Positron Annihilation (ICPA-13), Kyoto, Japan, 7 – 12 Sep. 2003. Abstract available.

Eldrup, M., Detection and characterisation of defects in metals and molecular solids by positron and positronium trapping. KFKI, Budapest, Hungary, 27 Oct. 2003. Unpublished.

Eldrup, M., Vacancy and vacancy clusters in metals and alloys. Positron Annihilation CNRS SCHOOL, CERI-CNRS, Orléans, France, 20 Nov. 2003. Unpublished.

Eldrup, M.; Singh, B.N.; Jung, P.; Jacquet, P., Effect of He on cavity formations in neutron irradiated iron and EUROFER-97. 11. International conference on fusion reactor materials (ICFRM-11), Kyoto (JP), 7-12 Dec 2003. Unpublished.

Ghoniem, N.M.; Wen, M.; Singh, B.N., Dislocation loop rafts and decoration in irradiated metals: Experimental evidence and computer simulations. 11. International conference on fusion reactor materials (ICFRM-11), Kyoto (JP), 7-12 Dec 2003. Unpublished.

Li, M.; Singh, B.N.; Stubbins, J.F., Room temperature creep-fatigue response of selected copper alloys for high heat flux applications. 11. International conference on fusion reactor materials (ICFRM-11), Kyoto (JP), 7-12 Dec 2003. Unpublished.

Osetsky, Y.N.; Bacon, D.J.; Singh, B.N., Atomic-scale dynamics of dislocation interaction with vacancy agglomerates in neutron irradiated bcc iron. TMS 2003 annual meeting: Symposium on microstructural processes in irradiated materials, San Diego (US), 3-6 Mar 2003. Unpublished. Abstract available

Osetsky, Y.N.; Bacon, D.J.; Singh, B.N., Dynamic properties of edge dislocations decorated by interstitial loops in a-Fe. TMS 2003 annual meeting: Symposium on microstructural processes in irradiated materials, San Diego (US), 3-6 Mar 2003. Unpublished. Abstract available

Peacock, A.T.; Barabash, V.; Dänner, W.; Linke, J.; Lorenzetto, P.; Marmy, P.; Merola, M.; Singh, B.N.; Tähtinen, S.; Laan, J. van der; Wu, C., Overview of recent European materials R and D for ITER and future perspectives. 11. International conference on fusion reactor materials (ICFRM-11), Kyoto (JP), 7-12 Dec 2003. Unpublished.

Schäblin, R.; Eldrup, M.; Singh, B.N.; Kohlbrecher, J.; Spätig, P.; Victoria, M., Identification of cavities in EUROFER irradiated at low dose. 11. International conference on fusion reactor materials (ICFRM-11), Kyoto (JP), 7-12 Dec 2003. Unpublished.

Singh, B.N., Deformation behaviour of OFHC copper under dynamic condition of displacement damage and plastic deformation. European fusion materials meeting, Garching (DE), 8-9 Apr 2003. Unpublished.

Singh, B.N., Deformation behaviour of copper alloys under creep-fatigue conditions. European fusion materials meeting, Garching (DE), 8-9 Apr 2003. Unpublished.

Singh, B.N., Effect of heat treatment on precipitate microstructure and mechanical properties of CuCrZr alloy in unirradiated and irradiated conditions. European fusion materials meeting, Garching (DE), 8-9 Apr 2003. Unpublished.

Singh, B.N., Consequences of single and multiatomic displacements in crystalline solids: Theoretical considerations and predictions. IGCAR, Kalpakkam (IN), 14 Apr 2003. Unpublished.

Singh, B.N., Consequences of single and multiatomic displacements in crystalline solids: Experimental determination of specific effects and validation of theoretical predictions. IGCAR, Kalpakkam (IN), 15 Apr 2003. Unpublished.

Singh, B.N., In-reactor deformation experiments. Workshop on fundamental aspects of radiation damage, Pacific Northwest National Laboratory, Richland (US), 4-8 Sep 2003. Unpublished.

Singh, B.N., Annealing kinetics of SFTs formed during neutron irradiation at different temperatures to different doses. Workshop on fundamental aspects of radiation damage, Pacific Northwest National Laboratory, Richland (US), 4-8 Sep 2003. Unpublished.

Singh, B.N., Global microstructural evolution and total response of materials exposed simultaneously to stress and irradiation producing displacement cascades. Workshop on fundamental aspects of radiation damage, Pacific Northwest National Laboratory, Richland (US), 4-8 Sep 2003. Unpublished.

Singh, B.N., Long term collaboration with Max Victoria. Seminar in the honour of Max Victoria, EPFL, Lausanne (CH), 20 Nov 2003. Unpublished.

Singh, B.N.; Edwards, D.J.; Tähtinen, S.; Moilanen, P.; Jacquet, P.; Dekeyser, J., Deformation behaviour of pore copper during in-reactor tensile tests at 90 deg C. 11. International conference on fusion reactor materials (ICFRM-11), Kyoto (JP), 7-12 Dec 2003. Unpublished.

Singh, B.N.; Golubov, S.I.; Trinkaus, H.; Edwards, D.J.; Eldrup, M., Evolution of stacking fault tetrahedra and its role in defect accumulation under cascade damage conditions. 11. International conference on fusion reactor materials (ICFRM-11), Kyoto (JP), 7-12 Dec 2003. Unpublished.

Trinkaus, H.; Singh, B.N., 1-D to 3-D diffusion reaction kinetics of cascade induced SIA clusters in metals: Implications for void nucleation and growth. TMS 2003 annual meeting: Symposium on microstructural processes in irradiated materials, San Diego (US), 3-6 Mar 2003. Unpublished. Abstract available

Trinkaus, H.; Singh, B.N.; Golubov, S.I., Impact of changes in 1-D diffusion direction and transversal diffusion of SIA clusters on damage accumulation in metals. 11. International conference on fusion reactor materials (ICFRM-11), Kyoto (JP), 7-12 Dec 2003. Unpublished.

Bibliographic Data Sheet **Risø-R-1468(EN)**

Title and authors

Association Euratom – Risø National Laboratory
Annual Progress Report 2003

Edited by H. Bindslev and B.N. Singh

ISBN	ISSN
87-550-3347-4 (Internet)	0106-2840; 1396-3449

Department or group	Date
Optics and Fluid Dynamics Department	May 2004

Pages	Tables	Illustrations	References
59	1	39	16

Abstract (max. 2000 characters)

Abstract The programme of the Research Unit of the Fusion Association Euratom - Risø National Laboratory covers work in fusion plasma physics and in fusion technology. The fusion plasma physics research focuses on turbulence and transport, and its interaction with the plasma equilibrium and particles. The effort includes both first principles based modelling, and experimental observations of turbulence and of fast ion dynamics by collective Thomson scattering. The activities in technology cover investigations of radiation damage of fusion reactor materials. These activities contribute to the Next Step, the Long-term and the Underlying Fusion Technology programme. A summary is presented of the results obtained in the Research Unit during 2003.

Descriptors INIS/EDB

CHARGED-PARTICLE TRANSPORT; ENERGY TRANSFER; MAGNETIC CONFINEMENT; NONLINEAR PROBLEMS; PHYSICAL RADIATION EFFECTS; PLASMA DIAGNOSTICS; PLASMA SIMULATION; PROGRESS REPORT; RISOE NATIONAL LABORATORY; THERMONUCLEAR REACTIONS; THERMONUCLEAR REACTOR MATERIALS; THOMSON SCATTERING; TOKAMAK DEVICES; TURBULENCE